

# Anti-tuberculosis Compound Screen using a Zebrafish Infection Model identifies an Aspartyl-tRNA Synthetase Inhibitor

Eva Habjan<sup>1,2</sup>, Vien QT Ho<sup>1</sup>, James Gallant<sup>2</sup>, Gunny Van Stempvoort<sup>2</sup>,  
Kin Ki Jim<sup>1</sup>, Coen Kuijl<sup>1</sup>, Daan P. Geerke<sup>3</sup>, Wilbert Bitter<sup>1,2</sup>,  
Alexander Speer<sup>1\*</sup>

<sup>1</sup> Department of Medical Microbiology and Infection Control, Amsterdam UMC, Location VU Medical Center, De Boelelaan 1108, 1081 HZ Amsterdam, The Netherlands

<sup>2</sup> Section Molecular Microbiology, Amsterdam Institute of Molecular and Life Sciences (AIMMS), Vrije Universiteit Amsterdam, De Boelelaan 1108, 1081 HZ Amsterdam, The Netherlands

<sup>3</sup> Department of Molecular Toxicology, Amsterdam Institute of Molecular and Life Sciences (AIMMS), Vrije Universiteit Amsterdam, De Boelelaan 1108, 1081 HZ Amsterdam, The Netherlands

\* Corresponding author: E-mail: [a.speer@amsterdamumc.nl](mailto:a.speer@amsterdamumc.nl)

**Keywords:** Mycobacterium tuberculosis, Tuberculosis, Zebrafish, Infection model, Drug-screening, Aminoacyl-tRNA synthetase

## Summary statement

This study used a zebrafish embryo infection model of tuberculosis to screen compounds for their *in vivo* activity. One of the hit compounds was characterized as an aspartyl-tRNA synthetase inhibitor.

## Abstract

Finding new anti-tuberculosis compounds with convincing *in vivo* activity is an ongoing global challenge to fight the emergence of multi-drug resistant *Mycobacterium tuberculosis* isolates. In this work, we exploited the medium-throughput capabilities of the zebrafish embryo infection model with *Mycobacterium marinum* as a surrogate for *M. tuberculosis*. Using a representative set of clinically established drugs, we demonstrate that this model could be predictive and selective for antibiotics that can be administered orally. We further used the zebrafish-infection model to screen 240 compounds from an anti-TB hit library for their *in vivo* activity and identified 14 highly active compounds. One of the most active compounds was the tetracyclic compound TBA161, which was studied in more detail. Analysis of resistant mutants revealed point mutations in *aspS* (*rv2572c*), encoding an aspartyl-tRNA synthetase. The target was genetically confirmed, and molecular docking studies propose possible binding of TBA161 in a pocket adjacent to the catalytic site. This study showed that the zebrafish-infection model is suitable to rapidly identify promising scaffolds with *in vivo* activity.

## Introduction

The disease tuberculosis (TB), caused by *Mycobacterium tuberculosis* (Mtb), is the deadliest bacterial infectious disease and is responsible for more than 1.5 million deaths annually (WHO, 2020a). Due to the emergence and increasing rate of multi and extensively drug-resistant strains, there is an urgent need to develop novel anti-tuberculosis drugs (Khawbung et al., 2021). Although drug discovery efforts have recently increased (Stop TB Partnership, 2019), the pre-clinical bottlenecks, such as *in vivo* efficacy testing, have limited the number of compounds reaching clinical studies (Koul et al., 2011a).

Numerous whole-cell based drug-screening campaigns yielded an extensive set of anti-mycobacterial compounds that are active *in vitro* against growing Mtb (Ananthan et al., 2009; Ballell et al., 2013; Maddry et al., 2009; Ollinger et al., 2019; Pethe et al., 2010). However, often promising compounds fail during *in vivo* studies due to unexpected toxicity and lack of *in vivo* efficacy (Ekins et al., 2014; Mukhopadhyay and Peterson, 2006; Pethe et al., 2010). The lack of efficacy is potentially attributed to the compound's unfavorable ADME (adsorption, distribution, metabolism, excretion) properties that cannot be sufficiently assessed during *in vitro* screens (Mukhopadhyay and Peterson, 2006; Pethe et al., 2010). *In vivo* studies that utilize traditional models such as rodents or primates are expensive, space- and time-consuming, labor-intensive, and ethically questionable as high-throughput screening models (Mukhopadhyay and Peterson, 2006; Singh and Gupta, 2018). Consequently, there is a need for alternative screening strategies to predict the safety and efficacy of drugs in mammalian models.

Previously, an early-life stage infection model of *Mycobacterium marinum* and zebrafish (*Danio rerio*) embryos was proposed to evaluate anti-tuberculosis compounds (Dalton et al., 2017; Ordas et al., 2015; Takaki et al., 2012). *M. marinum* is a close genetic relative to Mtb and is advantageous due to its shorter replication time and lower safety regulations (Biosafety level 2 organism) (Tobin and Ramakrishnan, 2008). While *M. marinum* causes opportunistic skin infection in humans, it is a natural pathogen of ectothermic animals, such as zebrafish, and causes tuberculosis-like disease (Jernigan and Farr, 2000). Additional advantages of using zebrafish embryos are their high fecundity, rapid development, and limited ethical constraints up to 120 hours post-fertilization (Cronan and Tobin, 2014). Moreover, due to the optical transparency of zebrafish embryos, infection progress can be easily followed in real-time (Davis et al., 2002). A steady increasing amount of studies and publications have proven and validated the *M. marinum*-zebrafish infection model to efficiently model mycobacterial pathogenesis (Lesley and Ramakrishnan, 2008; Prouty et al., 2003; Van Der Sar et al., 2004) and the host's innate immune response (Benard et al., 2016; Meijer et al., 2005; Van Der Vaart et al., 2012). Notably, the formation of hypoxic and necrotic granulomatous lesions was reported in infected zebrafish (Davis et al., 2002; Stoop et al., 2011), which is one of the hallmarks of human infection with Mtb.

Furthermore, zebrafish embryos were used to evaluate the efficacy and toxicity of several anti-tuberculosis drugs (Ho et al., 2021; Makarov et al., 2014; Ordas et al., 2015), including PBTZ169 (macozinone), which is currently in phase 2 clinical trial. The *M. marinum*-zebrafish model can be established by injecting bacteria via caudal vein or by injection in the yolk. Caudal

vein injections require precision and are therefore done manually, which is a labor-intensive endeavor allowing for hundreds of injections per day (Davis et al., 2002). Conversely, yolk injections can be performed with an automated robotic system, resulting in 1,000 infected embryos per hour (Carvalho et al., 2011; Ordas et al., 2015; Veneman et al., 2014; Wang et al., 2007). Furthermore, we show that the waterborne treatment of infected embryos allows the selection of active compounds that are absorbable through the zebrafish skin, which we determined to correlate with the oral uptake of antibiotics in humans. This is an important consideration since oral bioavailability is an essential prerequisite for novel anti-tuberculosis drugs, aiming to improve the current tuberculosis treatment regimens (WHO, 2020b).

In the present work, we optimized the previously described robotic yolk injection procedure in zebrafish (Ordas et al., 2015) to achieve higher throughput with the same reliability. We further used the platform to rapidly screen and identify anti-mycobacterial compounds and scaffolds that show excellent *in vivo* activity. Among our hits, we characterized a novel compound targeting the mycobacterial aspartyl-tRNA synthetase (AspS).

## Results

### Developing a medium-throughput *in vivo* screen

Previous studies have established the automated yolk injection procedure in zebrafish embryos using a robotic system (Carvalho et al., 2011; Ordas et al., 2015; Wang et al., 2007). In our study, we aimed to optimize the protocol in order to conduct a medium-throughput screen (MTS) of anti-mycobacterial compounds (Fig. 1A). We used an automated robotic micro-injector to inject fluorescently labeled *M. marinum* into the yolk of fertilized zebrafish embryos. Although the robotic yolk injection is fairly accurate, not all embryos are successfully injected. In order to efficiently select for correctly injected embryos, we mixed the bacterial suspension with the green-fluorescent dye fluorescein and injected the mixture into the zebrafish yolk. Fluorescein allowed for visualization of the injection procedure in real-time and rapid selection of injected embryos based on the green-fluorescent signal. The signal of fluorescein did not interfere with the red fluorescent signal that represents the bacterial load (Fig. S1A), and only green-positive embryos were subjected to analysis.

Next, we examined how different infection time-points affect bacterial localization within the zebrafish. When embryos were infected at the 2-32 cellular stage, the bacterial aggregates were detected in the yolk, head, tail, and body of the zebrafish, which is also observed after the caudal vein infection (Fig. S1B) and is established in the field to represent early granulomas (Davis et al., 2002; Stoop et al., 2011). Conversely, yolk infection at the 64 - 512 cellular stage resulted in bacterial accumulation exclusively in the yolk (Fig. S1B). Consequently, to achieve systemic infection, the zebrafish yolk-infection was consistently performed at no later than the 32-cellular stage.

Injection of approximately 100-150 colony-forming units (CFUs) resulted in a peak of infection at four days post-infection (dpi), and prolonged incubation resulted in the death of infected embryos. Since our goal was to quantify the infection levels per embryo, the treatment readout was at 4 dpi. Additionally, this time-point allowed us to discriminate between toxic and non-toxic compounds based on the early lethality or phenotypical changes of embryos in each treatment group (Fig. 1B).

### **Zebrafish infection model can predict oral bioavailability of tested compounds**

To validate our optimized *in vivo* screening approach, we tested several anti-tuberculosis drugs that are currently available or in clinical trials. Treatment of infected embryos was performed by adding the drugs directly into the fish water. This drug administration route is straightforward and highly suitable for MTS. All drugs were tested at a single concentration of 10  $\mu\text{M}$ , except for macozinone (1  $\mu\text{M}$ ) and ethionamide (5  $\mu\text{M}$ ), which were, due to toxicity, tested at lower concentrations. On 3 dpi, the bacterial load in each embryo was quantified using integrated red-fluorescent pixel intensity as a readout. Treatment with macozinone, sutezolid, bedaquiline, ethionamide, rifampicin, delamanid, pretonamid, and SQ109 showed a significant reduction of the bacterial signal (Fig. 1C). However, treatment with the approved anti-tuberculosis drugs streptomycin, kanamycin, linezolid, and levofloxacin at 10  $\mu\text{M}$  did not reduce the bacterial load in infected embryos. The infection levels were comparable to the levels of control treatment with the solvent DMSO (Fig. 1C).

Our initial set-up for drug testing only determined the antibacterial activity at a constant concentration of 10  $\mu\text{M}$  of an antibiotic, a concentration that is widely used for drug screening campaigns to select for highly active and specific hits. We investigated if levofloxacin, linezolid, kanamycin, and streptomycin would show antibacterial activity if tested at higher concentrations

in a zebrafish-infection survival assay. The treatment of infected zebrafish embryos was based on the antibiotics' minimum inhibitory concentration (MIC) determined in culture (Table S1). A concentration series from 25x to 400x MIC of the different antibiotics was added to the fish water at 1 dpi, and the survival of the embryos was analyzed at 4 dpi. We observed a dose-dependent increase in zebrafish survival when treated with linezolid or levofloxacin (Fig. 1D).

Conversely, the antibiotics kanamycin and streptomycin showed no activity even at 400x of the MIC value (Fig. 1D). We speculated that the inactivity might be due to poor uptake of the compound into the zebrafish embryo. Hence, we injected the compounds via the caudal vein at 1 dpi and observed a significant decrease in the bacterial load (Fig. S2A). These results demonstrate that streptomycin and kanamycin can reduce the infection in zebrafish, but only when injected directly into the bloodstream. The antibiotics streptomycin and kanamycin are clinically well established and effectively treating TB in patients. However, both antibiotics are administered via intravenous or intramuscular injections; hence, we postulated that the zebrafish model could predict the oral bioavailability of the tested compounds if compounds were administered into the fish water.

To test this hypothesis on a broader scale, we used the zebrafish embryo infection model with Gram-negative bacteria *Escherichia coli* and Gram-positive bacteria *Streptococcus pneumoniae* as infectious agents and different beta-lactam antibiotics that are either used for oral treatment (ceftibuten, cefixime and penicillin) or by intravenous injection (ceftazidime, ceftriaxone and meropenem). We chose this antibiotic class because it consists of several drugs that are comparable in their mode of action and differ mainly in their administration route. As a control treatment, we included the oral drug levofloxacin, a second-generation fluoroquinolone. Zebrafish embryos were infected via caudal vein injection route at 30 hours post-fertilization (hpf) with *E. coli* GK1161434 or *S. pneumoniae* D39V. A concentration range from 1x to 400x *in vitro* MIC (Table S1) of the different antibiotics was added to the fish water 1 hpf, and the survival of the embryos was analyzed 24 hours post-treatment (hpt). We observed a dose-dependent survival of infected embryos when treated with levofloxacin, ceftibuten, cefixime, and penicillin, whereas the non-treated groups showed a survival below 10% for both pathogens (Fig. 1E, F).

Interestingly, incubation with increasing concentration of ceftazidime, ceftriaxone, or meropenem did not increase the embryos' survival (Fig. 1E, F). Since these drugs are clinically administrated as intravenous injections, we investigated their curative potential when injected into the zebrafish. The treatment of *S. pneumoniae* infected embryos by intravenous injections

of 1x or 10x MIC of ceftazidime or meropenem resulted in 100% zebrafish survival (Fig. S2B). Treatment with ceftriaxone needed a concentration of 10x the MIC to obtain 90% survival of *S. pneumoniae* infected embryos (Fig. S2B). Similar results were obtained for ceftriaxone treatment of *E. coli* infected embryos (Fig. S2C).

Collectively, our results suggest that antibiotics that are clinically administered via intravenous injections show activity only when injected into the zebrafish bloodstream. Conversely, the antibiotics that are clinically administered as oral drugs showed activity when added to the fish water. Hence, our results suggest that the waterborne treatment of infected zebrafish embryos during a screen selects compounds with an increased chance of having good oral availability.

### **Medium-throughput screening of anti-Mtb library against *M. marinum* infected zebrafish embryos**

After the set-up of the *in vivo* screening approach, the platform was used to screen compounds of an anti-Mtb hit library (provided by TBAlliance (TBA)) for their *in vivo* activity. This library comprises 1392 compounds previously shown to inhibit Mtb viability *in vitro* (Ho et al., 2021). All compounds that showed  $\geq 80\%$  inhibition of *M. marinum* viability *in vitro* at 10  $\mu\text{M}$  (240 compounds) were selected and further tested in zebrafish-*M. marinum* infection model via automated yolk-injection and waterborne treatment using a single dose (10  $\mu\text{M}$ ) (Fig. 2A). From 240 tested compounds, 91 compounds exhibited toxic or lethal activity towards zebrafish embryos at 10  $\mu\text{M}$  and were excluded from further experiments and analysis. Among the 149 non-toxic compounds, we identified 14 compounds that significantly reduced bacterial load in infected zebrafish, the majority in a dose-dependent manner (Fig. 2B). Taken together, only 6% of compounds that were active against *M. marinum* in culture showed significant activity in the early *in vivo* zebrafish infection model, thus highlighting the translational gap between *in vitro* and *in vivo* models.

## ***In vivo* activity of compounds cannot be predicted from their physicochemical properties**

Our screen showed that *in vitro* activity of compounds does not translate directly to *in vivo* activity in an infection model. We examined whether *in vivo* activity in the zebrafish infection model could be predicted from the physicochemical properties of the compounds and collected those properties from online chemical databases (PubChem, ChemInfo) for the non-toxic test compounds (Table S7). The compounds were divided into three groups based on their activity in our model: (I) non-active compounds, (II) active compounds, (III) active reference antibiotics (macozinone, sutezolid, bedaquiline, ethionamide, rifampicin, delamanid, SQ109, pretonamid). Next, we performed a principal component analysis (PCA) to investigate if the correlation between those physicochemical properties can be used as a predictive model for the compounds' activity. None of the investigated chemical properties or their combinations showed clustering with the compounds' activity class (Fig. S3A), indicating that the compounds' activity in the zebrafish infection model cannot be predicted solely on their physicochemical properties. Interestingly, even approved antibiotics did not cluster and showed high variability (Fig. S3A). Although we did not observe clustering of the compounds' activity groups, the active compounds identified in this study show more variations in PC2 as compared to PC1 (Fig. S3A). We observed that the 14 identified active compounds show a lower molecular weight and lower complexity as compared to all 135 non-active compounds and approved antibiotics investigated in this study (Fig. S3B). The complexity value estimates the complexity of the molecule based on its composing elements and structural features (e.g., symmetry) while excluding the molecular stereochemistry (Bertz, 2002; Hendrickson et al., 1987). The current analysis was, however, limited to a large number of inactive compounds compared to a limited number of active compounds. Therefore, we cannot exclude that with more stratifying features and additional active compounds, predictive traits could be extracted.

## **Anti-bacterial characterization of 14 hit compounds**

We further characterized the 14 hit compounds from the *in vivo* screen by examining their activity in *in vitro* and *ex vivo* assays (Table 1). Compounds were tested against Mtb viability *in vitro*, and all of them showed dose-dependent activity with MIC<sub>50</sub> values below 10 µM (Table 1). Next, the compounds were tested against Mtb-infected THP-1 macrophages. In this *ex-vivo* model, the majority of the compounds showed dose-dependent intracellular activity by reducing



the bacterial viability while protecting macrophages from bacterial-induced lysis (Table 1 and Fig. S4). However, two compounds, TBA61 and TBA172, did not show activity in this model, whereas they were active against Mtb in culture and in the zebrafish-*M. marinum* infection model (Table 1 and Figs 2B,S4). Perhaps these compounds are mainly active against extracellular mycobacteria.

Most of the identified hit compounds have been previously described in the literature. For 13 compounds or their close derivatives, either the target was confirmed, or the mechanism of action was proposed based on genetic screens (Table 1). However, the mode of action of hit compound TBA161 was unknown. This compound was among the 4 most active compounds during fish infection experiments (Fig. 2B). Consequently, we decided to investigate this compound in more detail.

### **Characterization of TBA161 variants identifies a *meta*-di-chloro substituted derivative with higher activity**

The structure of compound TBA161 is comprised of four linear fused six-membered substituted heteroatom rings. The two outermost rings are a chloro-substituted benzyl ring and a thiazine on the opposite side of the structure. We obtained four derivatives with alteration in those two ring structures to investigate whether we could identify a more potent compound or find the compound's structural limitations towards activity (Table 2). The original compound TBA161 is a heterocyclic compound characterized by a single chloride atom on a benzyl ring. TBA161-A comprises a benzyl ring without any substitutes, whereas the derivative TBA161-B differs from the initial compound TBA161 by containing a bromo-benzyl. Compound TBA161-C is characterized by a double substituted *meta*-di-chlorobenzyl, and in the derivative TBA161-D the thiazine ring was opened.

All derivatives were tested for their activity against Mtb and *M. marinum* in culture. The compound with the most potent activity against both bacteria was TBA161-C, while TBA161-B and TBA161-A showed similar activity as the initial derivative TBA161 (Table 2). Inactivity of the TBA161-D indicates that the thiazine ring is crucial for the activity (Table 2). Next, the TBA161 derivatives that showed activity against Mtb in culture were investigated for intracellular activity using Mtb-infected THP-1 macrophages. All compounds inhibited bacterial growth and protected the Mtb-infected macrophages from lysis in a dose-dependent manner (Fig. 3A, B and Table 2).

The compounds were further investigated for their *in vivo* activity in the zebrafish-*M. marinum* infection model. The results were in line with the *in vitro* data, *i.e.*, all derivatives except TBA161-D showed a significant reduction of bacterial load in a dose-dependent manner, with TBA161-C being the most active compound (Fig. 3C, D). This was additionally confirmed during a zebrafish infection survival experiment, where embryos were yolk-infected with a high number of bacteria (1000 CFU), and the treatment efficacy was scored based on the zebrafish's survival (Fig. 3E). Compound TBA161-C showed the highest protective efficacy among the TBA161 derivatives (Fig. 3E). Consequently, the results are in agreement with previous *in vitro* and *in vivo* data (Fig. 3C,D and Table 2). We can conclude that the opening of the thiazine ring results in complete loss of *in vitro* and *in vivo* activity, whereas additional substitution of the benzyl ring to a *meta*-di-chloro-benzyl significantly increases the activity. All further experiments were performed with the most active derivative TBA161-C.

We tested TBA161-C against various bacterial strains to determine its specificity, but we only observed activity towards the slow-growing mycobacteria *M. marinum* and Mtb (Table S2). Moreover, TBA161-C was not cytotoxic to THP-1 monocytes and RAW 264.7 macrophages up to 40  $\mu$ M and zebrafish embryos up to 100  $\mu$ M (Table S2), thus confirming selective activity and a favorable safety profile.

### **Spontaneous resistant strains of *M. marinum* and *M. tuberculosis* carry mutations in the gene *aspS***

To identify the target of TBA161-C, we raised spontaneous resistant mutants of Mtb and *M. marinum*. Bacteria were continuously passaged in liquid culture with increasing concentrations of TBA161-C at every passage, resulting in the gradual selection of resistant strains. Single isolates were tested for their susceptibility towards TBA161-C. Both *M. marinum* and Mtb TBA161-C resistant strains showed MIC<sub>90</sub> exceeding 20  $\mu$ M, which is more than 10-fold higher as compared to the parental strains (Fig. 4A, B). The genomes of three resistant *M. marinum* strains were sequenced and compared to the parental strain. We identified in all resistant isolates the identical two single nucleotide polymorphisms (Table S3A). One of the mutations was located in *mmpL13* (MMAR\_4305), resulting in an amino acid substitution P502R. MmpL13 is a conserved transmembrane protein with an unknown function. The second mutation was located in *aspS* (MMAR\_2158), causing the amino acid substitution R168G. This gene is coding for an aspartyl-tRNA(Asp/Asn) synthetase. According to transposon mutagenesis studies,

*mmpL13* is not an essential gene for Mtb or *M. marinum*, whereas *aspS* was shown to be essential in both species (Dejesus et al., 2017; Griffin et al., 2011; Weerdenburg et al., 2015). Thus, we hypothesized that *aspS* might be the molecular target of TBA161-C.

Next, we performed whole-genome sequencing of the TBA161-C resistant Mtb isolate. The analysis revealed mutations in the gene *aspS* (*rv2572c*), resulting in amino acid substitution F526L (Table S3B), indicating that AspS might be involved in TBA161-C resistance in *M. marinum* as well as Mtb. In addition, two gene deletions were found (Table S3B). First, the deletion of gene *rv0544c*, which encodes for a possible conserved transmembrane protein. The second was the deletion of *lprK* (*mce1E* or *rv0173*), a predicted surface lipoprotein. According to the literature, both *lprK* and *rv0544c* are not essential for Mtb *in vitro* growth (Dejesus et al., 2017; Griffin et al., 2011).

Since both *M. marinum* and Mtb resistant isolates shared mutations in *aspS*, we speculated that *aspS* is the most probable molecular target of TBA161-C. Additionally, we investigated if *aspS* mutations are also present in other TBA161-C resistant Mtb isolates. Amplification and sequencing of the gene *aspS* (*rv2572c*) in Mtb of four resistant isolates revealed that all strains carried an identical mutation in *aspS* resulting in amino acid substitution F526L.

### Genetic cross-complementation confirms TBA161 to target AspS

To confirm the contribution of the identified mutations to the TBA161-C resistance, a genetic approach was applied. First, we amplified and cloned the WT *aspS* and mutated genes of *M. marinum* and Mtb under control of the constitutive promoter  $p_{smyc}$  resulting in four expression vectors. The overexpression vectors encoding the WT (*aspS*<sub>Mtb</sub>) and mutated *aspS* (*aspS*<sub>Mtb</sub>F526L) genes of Mtb were transformed into *M. marinum* WT, and vice versa Mtb was transformed with the expression constructs of *aspS*<sub>Mmar</sub> and *aspS*<sub>Mmar</sub>R168G. Next, the MIC of all strains against TBA161-C was determined. In both organisms, overexpression of the mutated *aspS* gene caused complete resistance to TBA161-C, in *M. marinum* (MIC<sub>90</sub> >40  $\mu$ M) and in *M. tuberculosis* (MIC<sub>90</sub> >80  $\mu$ M). Conversely, the strains overexpressing WT *aspS* remained susceptible, but showed an increased MIC<sub>90</sub> compared to the WT strains (5-fold for *M. marinum* and *M. tuberculosis*) (Fig. 4C, D and Table 2). These results demonstrate that target overexpression itself is not the main cause of resistance.

Nevertheless, we lowered the expression of *aspS*<sub>Mtb</sub>F526L by integrating the same expression cassette into the genome using the mycobacteriophage L5 attachment site and vector pML1342 in *M. marinum*. This integrative vector was previously shown to have 12- to 25-fold lower expression compared to the episomal vectors (Huff et al., 2010). The susceptibility of the strain towards TBA161-C was investigated in MIC assay. We showed that even when integrated in the genome, the strain expressing *aspS*<sub>Mtb</sub>F526L was resistant against TBA161-C, with MIC<sub>90</sub> higher than 40  $\mu$ M (Fig. S5A).

Next, we investigated if other mutations found in the TBA161-C resistant isolates could contribute to bacterial resistance towards TBA161-C. The *mmpL* genes have been shown to facilitate the transport of lipids and drugs across the cell envelope (Briffotiaux et al., 2017; Grzegorzewicz et al., 2012a). To investigate the putative role of *mmpL13* in resistance to TBA161-C, we amplified and cloned *M. marinum* WT *mmpL13* and mutated *mmpL13* (P502R) under control of the constitutive promoter p<sub>smyc</sub> and transformed the vectors into *M. marinum* WT. The effect of TBA161-C on *mmpL13* overexpressing strains was studied in the MIC assay. We found that the overexpression of WT or mutated *mmpL13* did not affect the susceptibility of the strains towards TBA161-C (Fig. S5B). Therefore, indicating that TBA161-C resistance in the isolated *M. marinum* mutant is primarily driven through a mutation in *aspS*. At this point, we cannot exclude that the deletions (frameshift mutations) of genes *rv0544c* and *rv0173* in Mtb contribute to resistance to TBA161-C. Future investigations will have to clarify this question. Collectively, our genetic cross-complementation approach confirmed that TBA161-C targets the aspartyl-tRNA(Asp/Asn) synthetase (*aspS*) in *M. marinum* and Mtb. Additionally, the TBA161-C resistant mutant of *M. marinum* displayed cross-resistance to the derivatives TBA161-A and TBA161-B, suggesting that those compounds have the same target (Fig. S6).

### **Molecular docking proposes possible binding of TBA161-C to *aspS***

Using molecular docking, we obtained binding poses of TBA161-C in Mtb *aspS* in which the central rings of the compound are in direct contact with residue R171 (R168 in *M. marinum*). Fig. 4E shows one of these poses and highlights other Mtb *aspS* residues that are in close vicinity of the compound, including T173, P174, F201, L204 and F519, and T570 of chain B of the 5W25 template structure. These residues correspond to T168, P169, F196, L199, F514, and T565 of *M. smegmatis* *aspS* that were previously identified as interacting partners for the compound C1 (Fig. 5A) docked into *M. smegmatis* *aspS* by Gurcha et al. (Gurcha et al., 2014).

One of the chloro-substituents of TBA161-C is found in the apolar cavity formed by L200, F201, L204 and F521, while the other may be involved in interaction with the hydroxyl group of the T173 side chain (Fig. 4E). These favorable contacts may be on the basis of the higher activity of TBA161-C when compared to the TBA161 derivatives that contain only a single or no aromatic halogen. Our docking results do not offer a direct explanation for the lack of activity of TBA161-D when compared to the other variants (Table 2). In addition, Fig. 4E depicts residue F526 of *Mtb aspS*, which is at a distance of more than 1 nm from the docked compound and hence does not show interaction with TBA161-C.

### **TBA161-C is a potent AspS-inhibitor showing excellent *in vivo* activity**

Previous studies reported several distinct compounds as AspS inhibitors in mycobacteria. Compound C1 was proposed to be an AspS inhibitor by identifying mutations in *aspS* of C1-resistant *Mtb* strains (Ioerger et al., 2013). Another study identified the inhibitor GSK93A during an *in vitro* whole-cell based screen established to identify AspS inhibitors by screening a hit-library (Soto et al., 2018). Here, we compared the activity of these two AspS inhibitors with our newly identified compound TBA161-C. Interestingly, these compounds show diverse chemical structures with only minor similarities, demonstrated by a Tanimoto coefficient below 0.5 (Fig. 5A and Fig. S7A). First, we compared the compounds' *in vitro* activity against *Mtb*. C1 showed comparable activity to TBA161-C, with the MIC<sub>90</sub> value of 2.5 μM, whereas GSK93A activity was 15-fold lower (Fig. S7B). Compound C1 also inhibited the growth of *M. marinum* in culture, whereas GSK93A did not show activity up to 40 μM (Fig. S7C). Next, we compared TBA161-C, C1 and GSK93A in the zebrafish-*M. marinum* infection model (Fig. 5B). Compound GSK93A was toxic to zebrafish at 10 μM, with only 40% of embryos surviving at 4 dpf. Neither GSK93A nor C1 showed activity in the zebrafish infection model, whereas TBA161-C, as we had shown previously, caused a significant reduction of bacterial burden in infected embryos (Fig. 5B). By comparing different compounds with the same proposed target, we can conclude that TBA161-C is a highly active AspS inhibitor *in vivo*, based on our zebrafish embryo infection experiments.

## Discussion

One of the challenges in drug discovery is to rapidly identify compounds that show the most promising characteristics to move on into clinical trials (Koul et al., 2011a). Since clinical trials are costly, losing a lead compound in the process should be minimized (DiMasi et al., 2016). To improve the success rate of newly discovered compounds, emphasis has been placed on the predictive value of pre-clinical model systems (Koul et al., 2011b; Wicha et al., 2018).

Widely used high-throughput screening (HTS) platforms allowed large libraries of chemical compounds to be screened on growing bacteria or during macrophage infection studies (Abrahams and Besra, 2020). However, these models do not mimic any of the vital ADME aspects during drug development, which can ultimately lead to a failure of the compound. Therefore, the need to evaluate compounds in animal models remains. However, the HTS of compounds in the traditional mammalian models, like mice, guinea pigs, rabbits and non-human primates, seems nearly impossible (Singh and Gupta, 2018).

Our study aimed to incorporate the *in vivo* model at the earlier steps of the drug discovery route in order to select the compounds with the highest chance to be active in later mammalian models. We used the zebrafish-embryo model, which presents an intriguing middle ground by providing an early *in vivo* infection model for compound evaluation, as well as the ability for medium-throughput screening due to assay miniaturization and process automatization (Bouz and Al Hasawi, 2018; Ordas et al., 2015; Schulthess et al., 2018; Spaink et al., 2013; Takaki et al., 2012). During our study, we screened 240 compounds and showed that only 6% of *in vitro* active compounds exhibited activity in the zebrafish-infection model. Our initial drug screen was based on a single concentration (10  $\mu$ M) in order to rapidly screen and select highly active compounds. Therefore, the screen is not sensitive enough to identify drugs that are active at higher concentrations, as shown with linezolid and levofloxacin (Fig. 1C,D). Moreover, we tried to establish a mathematical prediction model for compounds' *in vivo* activity based on their physicochemical properties, but our efforts were unsuccessful. Previous studies reported similar negative results as well (Koul et al., 2011b; Lakshminarayana et al., 2015). The low yield of compounds with *in vivo* activity and the inability to predict favorable compounds point to the need for early *in vivo* models.

In the course of our study, we demonstrated that the waterborne treatment of infected fish with antibiotics correlates with the high oral bioavailability of approved antibiotics for humans. However, it remains to be seen how strong the correlation is for the novel hits identified during our screen. Oral drugs are highly desirable for future tuberculosis drug regimens (Seung and Hewison, 2019; WHO, 2020b). Currently, all current first-line anti-TB drugs are oral antibiotics (WHO, 2020b). The long treatment times of tuberculosis, especially drug-resistant tuberculosis, would drastically increase treatment costs and reduce patient compliance, causing once more risk of developing resistant strains if parenteral antibiotics are chosen (Mase and Chorba, 2019; Seung and Hewison, 2019; WHO, 2020b). Thus, a pre-clinical model with a predictive value for the oral bioavailability of drugs in humans would be highly advantageous. The oral cavity of zebrafish embryos opens at 72h post-fertilization; however, embryos obtain nutrients from the yolk sack until seven days post-fertilization (Kimmel et al., 1995). Thus, in the early days, the uptake of drugs by the zebrafish embryo is facilitated exclusively across the zebrafish skin (van Wijk et al., 2019; Van Wijk et al., 2019). It has been well established that compounds in adult zebrafish can be taken up across the skin, and these models are extensively used in toxicology and pharmacology (Barros et al., 2008; Cassar et al., 2020; Glover et al., 2013; Morikane et al., 2020; Van Wijk et al., 2019). It is tempting to speculate, that the process of drugs diffusing through the zebrafish skin appears to be similar to the antibiotic's passive uptake across the human intestinal epithelium. Nevertheless, to verify the specificity of the current screening platform, further validation of the hit compounds and their oral bioavailability is needed.

In order to translate the drug response from zebrafish to humans, the link between internal drug exposure and its response needs to be established (Morgan et al., 2012; van Wijk et al., 2020a). Our screening conditions are very stringent: one-time treatment at a single concentration, meaning that the compound needs to be relatively stable in water and tissue, absorbable in high-enough concentrations to reach the target tissue, and have sterilizing activity. Besides that, the metabolism of the compound within the zebrafish should be slow. However, one remaining question of our study is the internal drug concentration within the infected zebrafish. Recently, a proof-of-concept study from van Wijk *et al.* showed that the isoniazid concentration in blood was only 20% of the external drug concentration (van Wijk et al., 2020b). Using pharmacokinetic-pharmacodynamic modeling, the authors described the exposure-response relationship and concluded that the early bactericidal effect of isoniazid in human infections translates to the responses observed in the zebrafish model (van Wijk et al., 2020b). A similar study was performed on paracetamol, showing that blood concentrations in the embryo were only 10% of the external paracetamol concentration in the fish water (Van Wijk

et al., 2019). Furthermore, after determining the pharmacokinetic properties, the authors showed that absorption, distribution, and elimination correlate well with parameters found in higher vertebrates, including humans (Kantae et al., 2016; Van Wijk et al., 2019). Overall, based on previous reports and an increase in understanding of the zebrafish infection model's translational value, we believe that compounds that exhibit activity in the zebrafish infection model have a great potential to be effective in mammalian infection models. Notably, some of the compounds identified as the 14 hit compounds during our screen in the zebrafish-infection model were previously reported to show activity in a mouse infection model: a variant of TBA57 is active against *Mtb in vivo* (Christophe et al., 2009a); an optimized version of compound TBA8 was shown to be active against *M. abscessus in vivo* (De Groote et al., 2018) and TBA117 and TBA120 are both related to Telacebec (Q203). Telacebec has successfully completed phase 2 clinical trials to be developed as an oral TB-drug (de Jager et al., 2020).

One of the most active compounds in our study during zebrafish and macrophage infection experiments was TBA161. In this work, we identified and confirmed the aspartyl-tRNA synthetase (AspS or AspRS) to be the molecular target of this scaffold in mycobacteria. AspS is a class II aminoacyl-tRNA synthetases (aaRSs) (Guo and Schimmel, 2012). These are essential enzymes for protein synthesis, as they ligate the specific tRNA molecules to their designated amino acid (Ling et al., 2009). Generally, each aaRS enzyme recognizes a specific amino acid/tRNA pair. However, some prokaryotes, including mycobacteria, do not encode asparagine tRNA synthetase (AsnRS) and glutamine tRNA synthetase (GlnRS) (Paravisi et al., 2009; Woese et al., 2000). Instead, they possess non-discriminating AspS and Glutamyl tRNA synthetase (GluRS) that can, besides Asp/tRNA<sup>Asp</sup> and Glu/tRNA<sup>Glu</sup>, also catalyze the formation of Asn/tRNA<sup>Asn</sup> and Gln/tRNA<sup>Gln</sup> pairs, respectively (Paravisi et al., 2009; Woese et al., 2000). The aaRSs enzymes represent attractive drug targets (Agarwal and Nair, 2012; Hurdle et al., 2005) as several natural and synthetic compounds have been reported to inhibit different aaRSs (Hurdle et al., 2005). For example, Microcin C (McC) and Tobramycin were reported as natural products that inhibit bacterial AspS (Walter et al., 2002), and several synthetic compounds have been identified as AspS inhibitors in mycobacteria (Gurcha et al., 2014; Ioerger et al., 2013; Soto et al., 2018). The best-characterized inhibitor, Compound C1, was identified by analysis of mutations in *aspS* of C1-resistant *Mtb* strains (Ioerger et al., 2013). Although C1 and TBA161 are structurally very different, with Tanimoto coefficients below 0.5, we identified one out of two mutated residues (F526) to be identical in AspS<sub>Mtb</sub> (Ioerger et al., 2013). The outcomes of our docking studies showed that the residue F526 does not play a direct role in inhibitor binding, which was also demonstrated by Gurcha *et al.* for compound C1 (Gurcha et al., 2014). The



authors were able to show that in an adjacent subunit of AspS, residue T570 of AspS<sub>Mtb</sub> can contribute to the binding of compound C1 (Gurcha et al., 2014), which we found for TBA161-C as well. Gurcha *et al.* reasoned that mutation F526 could cause small conformational changes, which can ultimately weaken the interaction with AspS<sub>Mtb</sub> residues that are in direct contact with the binding compound (Gurcha et al., 2014). The same effect could contribute to a lower affinity of AspS<sub>F526L</sub> to TBA161-C and, therefore, resistance. Interestingly, the other residue that contributed to the TBA161-C resistance, R171 (R168<sub>Mar</sub>), is located in the binding pocket of AspS and can directly participate in the binding of the inhibitor as confirmed by docking. So far, no AspS mutation has been associated with the drug resistance in the TB clinical samples (Flandrois et al., 2014; Joshi et al., 2014). The general database of variants detected in TB clinical isolates reports about five AspS mutations (Joshi et al., 2014). Notably, these mutations are distinct from the ones associated with the C1 or TBA161-C resistance. Thus, the TBA161-C has the potential to become a clinically relevant drug.

Taken together, we identified an anti-mycobacterial inhibitor that targets the essential enzyme AspS within the protein translation pathway and shows excellent activity in the zebrafish infection model. Therefore, the TBA161 scaffold has a high potential for a new drug against Mtb. Moreover, this study demonstrates the importance of incorporating early *in vivo* models in the drug discovery pipeline, which will not only accelerate the drug discovery route but also increase its success, saving great costs and efforts.

## Material and Methods

### Bacterial strains, eukaryotic cell lines, culture conditions

All bacterial strains used in this study are listed in Table S4. *Mycobacterium marinum* M<sup>USA</sup> was routinely cultured at 30°C in Middlebrook 7H9 medium or on 7H10 agar (Difco) supplemented with 10% ADS (0.5% BSA, 0.2% dextrose, 0.085% sodium chloride) and 0.02% tyloxapol. *Mycobacterium tuberculosis* H37Rv, and *Mycobacterium abscessus* were grown in the same medium at 37°C. *Escherichia coli*, *Bacillus subtilis*, *Klebsiella pneumoniae*, *Acinetobacter baumannii* were cultured at 37°C in Luria-Bertani (LB; Difco) medium or on LB agar plates, supplemented with hygromycin (50 µg/mL) where appropriate. *Streptococcus pneumoniae* was grown at 37°C with 5% CO<sub>2</sub> in Todd-Hewitt Broth (Bacto) supplemented with 2% Yeast Extract (THY; Oxoid) or on Columbia agar plates with 5% sheep blood (COS;

Biomerieux) supplemented with chloramphenicol (4.5 µg/mL) where appropriate. THP-1 human monocytes (ATCC® TIB-202™) were routinely cultured in RPMI medium with GlutaMAX™ (Gibco) supplemented with 10% fetal bovine serum (FBS) at 37°C with 5% CO<sub>2</sub>. RAW 264.7 murine macrophages (ATCC® TIB-71™) were routinely cultured in Dulbecco's modified Eagle's medium with GlutaMAX™ (DMEM; Gibco) supplemented with 10% FBS at 37°C with 5% CO<sub>2</sub>. Both cell lines were obtained from American Type Culture Collection (ATCC) and were passaged 5 times before a fresh culture is started. The tissue cultures are routinely controlled for mycoplasma contamination ever 3-6 months using a commercial kit based on PCR.

### Chemical reagents and compound library

Ceftibuten, cefixime, ceftazidime (hydrate), ceftriaxone (sodium), ethionamide, gentamycin, kanamycin (sulfate), levofloxacin, meropenem (trihydrate), penicillin (G sodium), rifampicin (all purchased from Sigma), bedaquiline, delamanid, linezolid, macozinone, pretonamid, streptomycin (sulfate salt), sutezolid, SQ109, TBA161 (9-Chloro-3,4-dihydro-chromeno[2',3':4,5]pyrimido[2,1-b][1,3]thiazine-6,7-dione) and its derivatives TBA161-A (3,4-dihydro-chromeno[2',3':4,5]pyrimido[2,1-b][1,3]thiazine-6,7-dione), TBA161-B (9-Bromo-3,4-dihydro-chromeno[2',3':4,5]pyrimido[2,1-b][1,3]thiazine-6,7-dione), TBA161-C (9,11-Dichloro-3,4-dihydro-chromeno[2',3':4,5]pyrimido[2,1-b][1,3]thiazine-6,7-dione) and TBA161-D (7-Chloro-3-isopropyl-2-(methylsulfanyl)-chromeno[2,3-d]pyrimidine-4,5-dione) were all purchased from MedChemExpress and solubilized and stored according to the manufacturers' recommendations.

The TB Alliance compound library was a gift from TBAlliance (New York, USA). The library consists of 1392 compounds that were previously shown to inhibit *M. tuberculosis* H37Rv viability *in vitro*. Compounds of this library were stored as stock solutions (10 mM) in DMSO at -80°C.

### Construction of plasmids and strains

All primers and plasmids used within this study can be found in Tables S5 and S6, respectively. Plasmids in this study were constructed using standard molecular cloning techniques summarized in Fig. S8.

## Bacterial susceptibility assays

Minimal inhibitory concentrations (MIC) against *Mycobacterium* species were determined using the resazurin reduction microplate assay (REMA) as previously described (Palomino et al., 2002). Briefly, selected compounds or antibiotics were 2-fold serial diluted in 96-well plates. Bacterial strains were grown to mid-logarithmic phase, harvested by centrifugation (3000 g, 10 min), washed in PBS supplemented with tyloxapol (0.02%), resuspended in growth medium and added to each well at the final OD<sub>600</sub> of 0.001. The lid of each plate was sealed with scotch tape and plates were incubated for 4 days at 30°C (*M. marinum*), 6 days at 37°C (*M. tuberculosis*), 2 days at 37°C (*M. abscessus*). Subsequently, 20 µL of resazurin solution (0.025% (w/v) resazurin sodium salt and 20% Tween 80 (ratio 3:1)) were added to each well. After the color conversion of the dye, bacterial viability was measured as fluorescence intensity using a BioTek plate reader (Synergy H1), bottom reading mode (excitation/emission; 560 nm/590 nm). When using a bacterial strain with a fluorescent marker (*M. marinum*-tdTomato), bacterial viability was either measured as fluorescence intensity of tdTomato signal (excitation/emission; 554 nm/581 nm), or the developed resazurin dye was transferred and analyzed in a new plate after the bacteria were pelleted in the 96-well plates (610 g, 5 min).

MICs against non-*Mycobacterium* species were determined using optical density (OD) measurements. After overnight growth, the bacterial cells were freshly diluted in an appropriate medium and grown at 37°C to mid-logarithmic phase. Selected compounds or antibiotics were 2-fold serial diluted in 96-well plates. Then, the cultures were harvested by centrifugation (3000 g rpm, 10 min), washed in PBS, and added to each well at the final OD<sub>600</sub> of 0.001. Plates were sealed and incubated at 37°C for 12 h with 3 mm continuous linear shaking in BioTek plate reader and the bacterial growth was measured as OD<sub>600</sub> every 15 min.

MICs against *S. pneumoniae* were determined using the REMA assay. Selected compounds or antibiotics were 2-fold serial diluted in 96-well plates. *S. pneumoniae* was grown in THY medium to mid-logarithmic phase and diluted to an OD<sub>600</sub> of 0.05 in each well of the 96-wells plate. Plates were incubated overnight at 37°C with 5% CO<sub>2</sub>. The following day 10 µL of 0.025% (w/v) resazurin sodium salt solution was added to each well and plates were incubated for 3 h at 37°C. Next, the fluorescence intensity was measured using a BioTek plate reader, bottom reading mode (excitation/emission; 560 nm/590 nm).

The data of each 96-well plate was normalized to DMSO treated wells (100% viability) after background subtraction. All compounds were tested in duplicates.

## Zebrafish (*Danio rerio*) maintenance

*Danio rerio* (zebrafish) used in this study were *casper* (*roy*<sup>a9/a9</sup>;*nac*<sup>w2/w2</sup>) compound homozygote mutant fish that completely lack all melanocytes and iridophores in both embryogenesis and adulthood (White et al., 2008). Adult fish were kept in recirculating tank systems at the Amsterdam Animal Research Center of the VU University under conditions of a 14 h/10 h light/dark cycle at pH 7.5 and 26°C according to standard protocols (zfin.org). Zebrafish care, breeding and experiments were performed in compliance with local animal welfare laws (Animal Experimental licensing Committee, DEC). All protocols adhered to the international guidelines specified by the EU Animal Protection Directive 86/609/EEC, which allows zebrafish embryos to be used up to the moment of free-living.

## Infection of zebrafish

Injection stocks of *M. marinum* M<sup>USA</sup>-*tdTomato* and *E. coli* GK1161434 were prepared in PBS with 20% glycerol, aliquoted and stored at -80°C. For injection of *S. pneumonia* D39V, a fresh culture was used. Before use, the injection stock was diluted 1:1 in PBS containing 0.17% (v/v) phenol red (Sigma) or 2.5 µg/mL fluorescein (Sigma) to aid visualization of the injection process. The number of injected bacteria was determined by plating injection volume of bacterial suspension on appropriate plates, followed by counting colony-forming units (CFU).

**Yolk infection:** Transparent *casper* (White et al., 2008) zebrafish embryos were infected using an automated microinjection system (Life Science Methods BV) as described previously (Spaink et al., 2013). Zebrafish embryos were infected 1 hour-post fertilization at 2-32 cell stage with 80-150 CFU/nL (1000 CFU/nL during survival experiments, Fig. 3E) of *M. marinum* M<sup>USA</sup>-*tdTomato* mixed with fluorescein (2.5 µg/mL in PBS). Successfully infected embryos were selected by detection of green-fluorescence and were incubated overnight at 31°C in E3 medium (5.0 mM NaCl, 0.17 mM KCl, 0.33 mM CaCl<sub>2</sub>\*2H<sub>2</sub>O, 0.33 mM MgCl<sub>2</sub>\*6H<sub>2</sub>O) supplemented with 0.3 mg/L methylene blue until antibiotic treatment.

**Caudal vein infection:** Transparent *casper* (White et al., 2008) zebrafish embryos were collected and incubated in E3 medium supplemented with 0.3 mg/L methylene blue. Prior to infection, embryos were mechanically dechorionated and anesthetized in 0.02 % (w/v) buffered 3-aminobenzoic acid methyl ester (pH 7.0) (Tricaine; Sigma-Aldrich, A5040). The zebrafish embryos were individually infected via the caudal vein route, as described elsewhere (Benard et al., 2012; Jim et al., 2016). Successfully infected embryos were collected and incubated at 28°C in E3 medium supplemented with 0.3 mg/L methylene blue until antibiotic treatment.

## Compound treatment of zebrafish

**Waterborne treatment:** One day post-infection of embryos with *M. marinum* M<sup>USA</sup>-*tdTomato* or one-hour post-infection with *E. coli* GK1161434 or *S. pneumoniae* D39, embryos were divided into treatment groups of 12-15 embryos per well. Embryos were treated with test compounds diluted in fish water (60 µg/mL instant ocean sea salts) and incubated at 28°C. The survival rate was determined daily based on the functioning of the embryos' heart and blood circulation.

**Intravenous injection:** At one day post-infection with *M. marinum* M<sup>USA</sup>-*tdTomato* or one hour post-infection with *E. coli* GK1161434 or *S. pneumoniae* D39V, zebrafish embryos were re-injected with 1 nL of different antibiotics at indicated concentrations. Infected and intravenously treated zebrafish were incubated in fish water at 28°C. The survival rate was determined daily based on heartbeat and blood circulation.

## Determination of bacterial load in infected zebrafish embryos

Three days after the treatment, the *M. marinum-tdTomato* infected zebrafish were anesthetized in 0.02 % (w/v) buffered 3-aminobenzoic acid methyl ester (pH 7.0) (Tricaine; Sigma-Aldrich), and the bacterial load was monitored with an Olympus IX83 fluorescence microscope (4x objective magnification, Hamamatsu ORCA-Flash 4.0 camera) at specific wavelengths (excitation/emission; 470 nm/519 nm; 550 nm/610 nm). Obtained images were analyzed using CellProfiler 3.19 (Broad Institute, Cambridge, USA) with a custom-made pipeline to count and quantify pixels intensity within the embryos. Integrated red fluorescence intensity

per embryo was used as a readout for bacterial burden. Image acquisition and image analysis were automated.

## **Zebrafish toxicity studies**

Transparent *casper* (White et al., 2008) zebrafish embryos were collected within the first hours post-fertilization and kept overnight at 31°C in E3 medium supplemented with 0.3 mg/L methylene blue. One day post-fertilization (dpf), zebrafish embryos were treated with compounds diluted in fish water at the indicated concentration. Zebrafish embryos were incubated at 28°C for 5 days, and the morphology and mortality of zebrafish embryos were monitored daily.

## **Generation and characterization of spontaneous TBA161-C resistant mutants**

Spontaneously resistant mutants of *M. marinum-tdTomato* or Mtb strains were generated using natural selection strategies. TBA161-C resistant mutants from both strains were isolated from 7H9 cultures over 5 passages with increasing concentrations of TBA161-C starting from 0.3x, 1x, 3x, 6x MIC to final concentrations of 10x MIC for *M. marinum* and Mtb. Single colonies were obtained by streaking cultures on 7H10 plates. The resistance to TBA161-C was determined by testing the susceptibility of strains to TBA161-C using the REMA assay. Genomic DNA extraction of TBA161-C resistant and parental mycobacterial strains was done using phenol/chloroform/isoamyl-alcohol extraction as described previously (Mve-Obiang et al., 2001). Whole-genome sequencing of genomic DNA from parental WT *M. marinum-tdTomato* and three TBA161-C resistant *M. marinum-tdTomato* strains were outsourced to Beijing Novogene Bioinformatics Technology Co., Ltd. (Novogene, China) using Illumina sequencing technology. Generated reads were aligned to the reference genome of *M. marinum* M<sup>USA</sup> (NC\_010612.1) and compared to the parental strain using the software Qiagen CLC Genomics Workbench 12 (QIAGEN, Aarhus, Denmark). TBA161-C resistant Mtb mutant strains were analyzed by Sanger sequencing after amplification of the *aspS* gene by PCR.

## Cytotoxicity

Compounds were distributed as two-fold serial dilutions in RPMI GlutaMAX™ with 10% FBS and incubated with THP-1 monocytes ( $2.5 \times 10^4$  cells/well) or in DMEM GlutaMAX™ with 10% FBS and incubated with RAW macrophages ( $2.5 \times 10^4$  cells/well) for 3 days at 37°C with 5% CO<sub>2</sub>. After incubation, resazurin sodium salt (0.0025% (w/v) in PBS) was added to wells, and plates were incubated for 4 h at 37°C. Cell viability was measured as fluorescent intensity using BioTek plate reader (excitation/emission; 560 nm/590 nm).

## Assessment of intracellular drug activity in infected THP-1 macrophages

Mtb transformed with pTetDuo was grown in 7H9 at 37°C to mid-logarithmic phase, then harvested and washed in PBS. Bacterial infection stocks were prepared in RPMI GlutaMAX™ with 10% FBS (infection medium) with 20% glycerol, aliquoted and stored at -80°C. THP-1 human monocytes were seeded into black 96-well plates (Ibidi) as  $10^5$  cells/well and incubated with phorbol-12-myristate-13-acetate (PMA) (25 ng/mL) for 48 h at 37°C with 5% CO<sub>2</sub> to induce differentiation to macrophage-like cells. Differentiated macrophages were washed in infection medium and then infected with Mtb H37Rv carrying pTetDuo at a multiplicity of infection (MOI) of 5. After 3 h incubation at 37°C with 5% CO<sub>2</sub>, extracellular bacteria were killed by the addition of gentamycin (50 µg/mL) for 1 h at 37°C with 5% CO<sub>2</sub>. After incubation, the medium was replaced with the test compounds, which were prepared in separate 96-well plates by 3-fold serial dilutions in infection medium. Plates were incubated for 4 days at 37°C with 5% CO<sub>2</sub>. After incubation, anhydrotetracycline (ATc) solution (100 ng/mL) in RPMI was added and plates were incubated for an additional 24 h at 37°C with 5% CO<sub>2</sub>. The medium was replaced with 160 µL of paraformaldehyde (3.2% (w/v)) in PBS, followed by incubation for 30 min at room temperature. The fixating solution replaced with 160 µL of quenching/staining solution (0.1 M glycine, 0.2% (w/v) Triton X-100, Hoechst dye 1:500 in PBS) was added and incubated for 1 h in the dark. All wells were washed two times with PBS. Olympus IX83 fluorescence microscope (20x objective magnification) with Hamamatsu ORCA-Flash 4.0 camera was used to acquire images of each well at specific wavelengths (excitation/emission; 385 nm/455 nm; 470 nm/519 nm; 550 nm/610 nm). Image analysis was done using CellProfiler 3.19 (Broad Institute, Cambridge, USA) with a custom-made pipeline that identifies the macrophages based on the blue Hoechst dye-stained macrophages nuclei. In order to account for the cytosol of the macrophage, the radius around the nuclei (median diameter 8.2 µm) was extended by 10 pixels without allowing overlap with

neighboring macrophages (median diameter 11.9  $\mu\text{m}$ ). The fluorescent signal of the ATc inducible GFP was used as a readout for viable intracellular bacteria in each macrophage. The number of stained and detected nuclei was used as a readout for the number of macrophages in each treatment group, and was normalized to rifampicin (3  $\mu\text{M}$ ) treated sample (100% macrophage viability). The average GFP signal in each treatment group was calculated and normalized on the control DMSO-treated sample (100% bacterial viability).

## Molecular docking

Chain A of crystal structure 5W25 (Dranow, D.M., Lorimer, D.D., Edwards, 2017) of *M. tuberculosis aspS* was protonated using the Molecular Operator Environment software (version 2019.09) (Chemical Computing Group ULC, 2021) and used as a template to dock compound TBA16-C into (after removal of crystal water molecules). Docking was performed using the Protein-Ligand ANT System (PLANTS, version 1.2) software (Korb et al., 2007) in combination with the ChemPLP scoring function (Korb et al., 2009). A two-step protocol was used to obtain the docking pose presented in this work. First, TBA161-C was docked into the binding pocket corresponding to the one described by Gurcha *et al.* in their structural characterization of *M. smegmatis aspS* (Gurcha et al., 2014), which is highly (82%) homologous to *M. tuberculosis aspS*. In this initial step, we set the center of docking close to R171 (R168 in *M. marinum*; i.e., at the center of the vector connecting CD1 of F519 with CG of R171), and the docking radius to 0.8 nm. Subsequently, we used the coordinates of one of the thus obtained poses with close contacts to R171 as starting point to further explore the binding pocket in a second docking run, in which a larger docking radius (1.0 nm) was used and the center of docking was set to the center of the vector connecting CG2 of T173 and HE2 of F456. To allow for an induced fit effect, we adapted the side-chain conformations of residues L200, F519 and F521 prior to this second docking run, by changing the CA-CB-CG-CD1 dihedral angles of L200 and F519 from 177.3 to  $-63.1$  degrees and  $-82.5$  to 59.0 degrees, respectively, and by changing the F521 C-CA-CB-CG dihedral angle from  $-58.9$  to  $-151.1$  degrees. The above mentioned Mtb *aspS* residues R171, T173, F456 and F519 are corresponding to *M. smegmatis aspS* residues aligning the binding pocket in which Gurcha *et al.* successfully docked compound C1 into, using their 4RMF crystal structure as docking template (Gurcha et al., 2014). The residues aligning this pocket are conserved between *aspS* of Mtb and *M. smegmatis* and show nearly identical backbone and side-chain conformations in both the 5W25 and 4RMF structures. To verify our docking



approach, we redocked C1 using our protocol into the 5W25 structure and obtained a similar binding pose as Gurcha *et al.*

## Principle component analysis (PCA)

Exploratory data analysis was conducted on data containing the physicochemical properties of compounds, which were either known for *in vitro* activity against Mtb and *M. marinum*. Compound's properties used for analysis were: molecular weight, logP, logS, polar surface area, XLogP3-AA, number of H-donors, number of H-acceptors, heavy atom number, number of rotatable bonds, complexity, number of NO<sub>2</sub> groups, number of S-atoms (Table S7). For imputation of missing values, data was assumed to be missing at random and were imputed using predictive mean matching from the MICE package using the R statistical programming language (van Buuren and Groothuis-Oudshoorn, 2011). The resulting imputed data frame was further z-scored and used for principal component analysis.

## Statistical analysis

All statistical analyses in this study were performed using GraphPad Prism version 9.0.0 (GraphPad Software Inc, San Diego, California, USA). The MIC<sub>50</sub> values representing 50% growth inhibition and MIC<sub>90</sub> values represent 90% growth inhibition. The MIC values were determined by generating dose-response curves using a nonlinear fitting of the data with a variable slope. The IC<sub>50</sub> (the half-maximal inhibitory concentration) and TD<sub>50</sub> (median toxic dose) values were calculated using the same equation.

The effect of drug treatment in infected zebrafish embryos was analyzed using integrated red-fluorescence intensity as a readout. Each data point represents a signal from a single zebrafish embryo and each treatment group consisted of minimum of 10 embryos. Embryos with a fluorescent intensity equal to 0 were set to 1 to allow log<sub>10</sub> transformation. Log<sub>10</sub> transformation was performed to achieve normal distribution. Further statistical analysis on log<sub>10</sub> transformed values was performed using a one-way ANOVA, following Dunnett's multiple comparison test by comparing the signal from the DMSO-treated control sample with each treatment group. Significance is indicated as: \*  $p \leq 0.05$ ; \*\*  $p \leq 0.01$ ; \*\*\*  $p \leq 0.001$ ; \*\*\*\*  $p \leq 0.0001$ .

## Acknowledgement

We want to thank TB Alliance and Nader Fotouhi for discussions and for providing us with the hit-compound library used in this study. Robert Stavenger (GSK) for sending us the *E. coli* strains used for fish experiments and Karin van Dijk (MMI, AmsterdamUMC), Oscar Kuipers (RUG), Jan-Willem Veening (UNIL) and Gina Schouten for sharing bacterial (clinical) isolates. We thank the Niederweis lab for the plasmids pMS2, pMN016, pMN437, pML1342, and pML2424 that we received as a gift. We would like to thank Astrid van der Sar for her help setting up the zebrafish work, Theo Verboom for support during the zebrafish experiments and Savannah Devente for helping during the initial compound screening experiments. We thank Joen Luijck, Christina Vandenbroucke-Grauls and Mark Rong for insightful discussions.

## Competing interests

The authors declare no competing interests.

## Funding

This work was supported by the Netherlands Organization for Scientific Research (NWO) through TTW-NACTAR-16445 granted to WB and the VENI grant (016.Veni.171.090) awarded to AS. The organization Amsterdam Infection and Immunity (AI&I) supported this work with funding awarded to AS. The research leading to these results has received funding from the Innovative Medicines Initiative Joint Undertaking under grant agreement n°115583, resources of which are composed of financial contribution from the European Union's Seventh Framework Program (FP7/2007-2013) and EFPIA companies' in kind contribution. The ENABLE project is also financially supported by contributions from Academic and SME partners.

## Data availability:

Whole genome sequencing data of WT and TBA161-C-resistant *M. marinum* and *M.tuberculosis* strains have been deposited to the Sequence Read Archive (SRA) within

BioProject PRJNA761549 (BioSample accession SAMN19006095) and PRJNA727079 (BioSample accession SAMN19006075, SAMN19006076, SAMN19006077, SAMN19006078).

## Authors contributions statement

E.H., V.Q.T.H., J.G., G.V.S., K.K.J, C.K., D.P.G, W.B., and A.S. conceptualized the research; E.H., V.Q.T.H., J.G., G.V.S., K.K.J, C.K., D.P.G, and A.S. performed investigation; E.H., V.Q.T.H., J.G., G.V.S., K.K.J, C.K., D.P.G, W.B., and A.S. performed validation and formal analysis; E.H., D.P.G, W.B., and A.S. wrote the original draft. All authors reviewed and edited the manuscript. W.B. and A.S. contributed with funding acquisition and project administration.

## References

- Abrahams, K. A. and Besra, G. S.** (2020). Mycobacterial drug discovery. *RSC Med. Chem.* **11**, 1354–1365.
- Agarwal, V. and Nair, S. K.** (2012). Aminoacyl tRNA synthetases as targets for antibiotic development. *Medchemcomm* **3**, 887–898.
- Ananthan, S., Faaleolea, E. R., Goldman, R. C., Hobrath, J. V., Kwong, C. D., Laughon, B. E., Maddry, J. A., Mehta, A., Rasmussen, L., Reynolds, R. C., et al.** (2009). High-throughput screening for inhibitors of Mycobacterium tuberculosis H37Rv. *Tuberculosis* **89**, 334–353.
- Arora, K., Ochoa-Montaño, B., Tsang, P. S., Blundell, T. L., Dawes, S. S., Mizrahi, V., Bayliss, T., Mackenzie, C. J., Cleghorn, L. A. T., Ray, P. C., et al.** (2014). Respiratory flexibility in response to inhibition of cytochrome C oxidase in Mycobacterium tuberculosis. *Antimicrob. Agents Chemother.* **58**, 6962–6965.
- Ballell, L., Bates, R. H., Young, R. J., Alvarez-Gomez, D., Alvarez-Ruiz, E., Barroso, V., Blanco, D., Crespo, B., Escribano, J., González, R., et al.** (2013). Fueling Open-Source Drug Discovery: 177 Small-Molecule Leads against Tuberculosis. *ChemMedChem* **8**, 313–321.
- Barros, T. P., Alderton, W. K., Reynolds, H. M., Roach, A. G. and Berghmans, S.** (2008). Zebrafish: An emerging technology for in vivo pharmacological assessment to identify potential safety liabilities in early drug discovery. *Br. J. Pharmacol.* **154**, 1400–1413.
- Benard, E. L., van der Sar, A. M., Ellett, F., Lieschke, G. J., Spaink, H. P. and Meijer, A. H.** (2012). Infection of zebrafish embryos with intracellular bacterial pathogens. *J. Vis. Exp.* **61**, 3781.
- Benard, E. L., Rougeot, J., Racz, P. I., Spaink, H. P. and Meijer, A. H.** (2016). Transcriptomic Approaches in the Zebrafish Model for Tuberculosis—Insights Into Host- and Pathogen-specific Determinants of the Innate Immune Response. *Adv. Genet.* **95**, 217–251.
- Bertz, S. H.** (2002). The first general index of molecular complexity. *J. Am. Chem. Soc.* **103**, 3599–3601.
- Bouz, G. and Al Hasawi, N.** (2018). The zebrafish model of tuberculosis - no lungs needed. *Crit. Rev. Microbiol.* **44**, 779–792.

- Briffotiaux, J., Huang, W., Wang, X. and Gicquel, B.** (2017). MmpS5/MmpL5 as an efflux pump in Mycobacterium species. *Tuberculosis (Edinb)*. **107**, 13–19.
- Brown, J. R., North, E. J., Hurdle, J. G., Morisseau, C., Scarborough, J. S., Sun, D., Korduláková, J., Scherman, M. S., Jones, V., Grzegorzewicz, A., et al.** (2011). The structure-activity relationship of urea derivatives as anti-tuberculosis agents. *Bioorganic Med. Chem.* **19**, 5585–5595.
- Carvalho, R., de Sonneville, J., Stockhammer, O. W., Savage, N. D. L., Veneman, W. J., Ottenhoff, T. H. M., Dirks, R. P., Meijer, A. H. and Spalink, H. P.** (2011). A high-throughput screen for tuberculosis progression. *PLoS One* **6**,.
- Cassar, S., Adatto, I., Freeman, J. L., Gamse, J. T., Iturria, I., Lawrence, C., Muriana, A., Peterson, R. T., Van Cruchten, S. and Zon, L. I.** (2020). Use of Zebrafish in Drug Discovery Toxicology. *Chem. Res. Toxicol.* **33**, 95–118.
- Chemical Computing Group ULC** (2021). Molecular Operating Environment (MOE), 2019.01.
- Christophe, T., Jackson, M., Jeon, H. K., Fenistein, D., Contreras-Dominguez, M., Kim, J., Genovesio, A., Carralot, J.-P., Ewann, F., Kim, E. H., et al.** (2009a). High Content Screening Identifies Decaprenyl-Phosphoribose 2' Epimerase as a Target for Intracellular Antimycobacterial Inhibitors. *PLoS Pathog.* **5**, e1000645.
- Christophe, T., Jackson, M., Jeon, H. K., Fenistein, D., Contreras-Dominguez, M., Kim, J., Genovesio, A., Carralot, J.-P., Ewann, F., Kim, E. H., et al.** (2009b). High Content Screening Identifies Decaprenyl-Phosphoribose 2' Epimerase as a Target for Intracellular Antimycobacterial Inhibitors. *PLoS Pathog.* **5**, e1000645.
- Cronan, M. R. and Tobin, D. M.** (2014). Fit for consumption: Zebrafish as a model for tuberculosis. *DMM Dis. Model. Mech.* **7**, 777–784.
- Dalton, J. P., Uy, B., Okuda, K. S., Hall, C. J., Denny, W. A., Crosier, P. S., Swift, S. and Wiles, S.** (2017). Screening of anti-mycobacterial compounds in a naturally infected zebrafish larvae model. *J. Antimicrob. Chemother.* **72**, 421–427.
- Davis, J. M., Clay, H., Lewis, J. L., Ghori, N., Herbomel, P. and Ramakrishnan, L.** (2002). Real-time visualization of Mycobacterium-macrophage interactions leading to initiation of granuloma formation in zebrafish embryos. *Immunity* **17**, 693–702.
- De Groote, M. A., Jackson, M., Gonzalez-Juarrero, M., Li, W., Young, C. L., Wong, C., Graham, J., Day, J., Hoang, T., Jarvis, T. C., et al.** (2018). Optimization and lead selection of benzothiazole amide analogs toward a novel antimycobacterial agent. *Front. Microbiol.* **9**, 2231.
- de Jager, V. R., Dawson, R., van Niekerk, C., Hutchings, J., Kim, J., Vanker, N., van der Merwe, L., Choi, J., Nam, K. and Diacon, A. H.** (2020). Telacebec (Q203), a New Antituberculosis Agent. *N. Engl. J. Med.* **382**, 1280–1281.
- Dejesus, M. A., Gerrick, E. R., Xu, W., Park, S. W., Long, J. E., Boutte, C. C., Rubin, E. J., Schnappinger, D., Ehrh, S., Fortune, S. M., et al.** (2017). Comprehensive essentiality analysis of the Mycobacterium tuberculosis genome via saturating transposon mutagenesis. *MBio* **8**,.
- DiMasi, J. A., Grabowski, H. G. and Hansen, R. W.** (2016). Innovation in the pharmaceutical industry: New estimates of R&D costs. *J. Health Econ.* **47**, 20–33.
- Dranow, D.M., Lorimer, D.D., Edwards, T. E.** (2017). RCSB PDB - 5W25: Crystal structure of Aspartyl-tRNA synthetase from Mycobacterium tuberculosis complexed with L-Aspartic Acid.

- Ekins, S., Nuermberger, E. L. and Freundlich, J. S.** (2014). Minding the gaps in tuberculosis research. *Drug Discov. Today* **19**, 1279–1282.
- Flandrois, J.-P., Lina, G. and Dumitrescu, O.** (2014). MUBII-TB-DB: a database of mutations associated with antibiotic resistance in *Mycobacterium tuberculosis*. *BMC Bioinforma.* 2014 151 **15**, 1–9.
- Glover, C. N., Bucking, C. and Wood, C. M.** (2013). The skin of fish as a transport epithelium: A review. *J. Comp. Physiol. B Biochem. Syst. Environ. Physiol.* **183**, 877–891.
- Graham, J., Wong, C. E., Day, J., McFaddin, E., Ochsner, U., Hoang, T., Young, C. L., Ribble, W., DeGroot, M. A., Jarvis, T., et al.** (2018). Discovery of benzothiazole amides as potent antimycobacterial agents. *Bioorganic Med. Chem. Lett.* **28**, 3177–3181.
- Griffin, J. E., Gawronski, J. D., Dejesus, M. A., Ioerger, T. R. and Akerley, B. J.** (2011). High-Resolution Phenotypic Profiling Defines Genes Essential for Mycobacterial Growth and Cholesterol Catabolism. *PLoS Pathog* **7**, 1002251.
- Grzegorzewicz, A. E., Pham, H., Gundi, V. A. K. B., Scherman, M. S., North, E. J., Hess, T., Jones, V., Gruppo, V., Born, S. E. M., Korduláková, J., et al.** (2012). Inhibition of mycolic acid transport across the *Mycobacterium tuberculosis* plasma membrane. *Nat. Chem. Biol.* **8**, 334–341.
- Guo, M. and Schimmel, P.** (2012). Structural analyses clarify the complex control of mistranslation by tRNA synthetases. *Curr. Opin. Struct. Biol.* **22**, 119–126.
- Gurcha, S. S., Usha, V., Cox, J. A. G., Fütterer, K. and Abrahams, K. A.** (2014). Biochemical and Structural Characterization of Mycobacterial Aspartyl-tRNA Synthetase AspS, a Promising TB Drug Target. *PLoS One* **9**.
- Hearn, M., Smaltz, D. and Cynamon, M.** (2014). Synthesis and Antitubercular Activities in Vitro of New p-Aminosalicylic Ester Imines. *Lett. Drug Des. Discov.* **11**, 953–959.
- Hendrickson, J. B., Huang, P. and Toczko, A. G.** (1987). Molecular Complexity: A Simplified Formula Adapted to Individual Atoms. *J. Chem. Inf. Comput. Sci.* **27**, 63–67.
- Ho, V. Q. T., Verboom, T., Rong, M. K., Habjan, E., Bitter, W. and Speer, A.** (2021). Heterologous expression of ethA and katG in *Mycobacterium marinum* enables the rapid identification of new prodrugs active against *Mycobacterium tuberculosis*. *Antimicrob. Agents Chemother.* **65**.
- Huff, J., Czyz, A., Landick, R. and Niederweis, M.** (2010). Taking phage integration to the next level as a genetic tool for mycobacteria. *Gene* **468**, 8–19.
- Hurdle, J. G., O'Neill, A. J. and Chopra, I.** (2005). Prospects for aminoacyl-tRNA synthetase inhibitors as new antimicrobial agents. *Antimicrob. Agents Chemother.* **49**, 4821–4833.
- Ioerger, T. R., O'Malley, T., Liao, R., Guinn, K. M., Hickey, M. J., Mohaideen, N., Murphy, K. C., Boshoff, H. I. M. M., Mizrahi, V., Rubin, E. J., et al.** (2013). Identification of New Drug Targets and Resistance Mechanisms in *Mycobacterium tuberculosis*. *PLoS One* **8**, e75245.
- Jernigan, J. A. and Farr, B. M.** (2000). Incubation period and sources of exposure for cutaneous *Mycobacterium marinum* infection: Case report and review of the literature. *Clin. Infect. Dis.* **31**, 439–443.

- Jim, K. K., Engelen-Lee, J. Y., van der Sar, A. M., Bitter, W., Brouwer, M. C., van der Ende, A., Veening, J. W., van de Beek, D. and Vandenbroucke-Grauls, C. M. J. E. (2016). Infection of zebrafish embryos with live fluorescent *Streptococcus pneumoniae* as a real-time pneumococcal meningitis model. *J. Neuroinflammation* **13**,.
- Johnson, E. O., LaVerriere, E., Office, E., Stanley, M., Meyer, E., Kawate, T., Gomez, J. E., Audette, R. E., Bandyopadhyay, N., Betancourt, N., et al. (2019). Large-scale chemical–genetics yields new *M. tuberculosis* inhibitor classes. *Nature* **571**, 72–78.
- Joshi, K. R., Dhiman, H. and Scaria, V. (2014). tbvar: a comprehensive genome variation resource for *Mycobacterium tuberculosis*. *Database* **2014**,.
- Kantae, V., Krekels, E. H. J., Ordas, A., González, O., Van Wijk, R. C., Harms, A. C., Racz, P. I., Van Der Graaf, P. H., Spaink, H. P. and Hankemeier, T. (2016). Pharmacokinetic modeling of paracetamol uptake and clearance in zebrafish larvae: Expanding the allometric scale in vertebrates with five orders of magnitude. *Zebrafish* **13**, 504–510.
- Khawbung, J. L., Nath, D. and Chakraborty, S. (2021). Drug resistant Tuberculosis: A review. *Comp. Immunol. Microbiol. Infect. Dis.* **74**, 101574.
- Kimmel, C. B., Ballard, W. W., Kimmel, S. R., Ullmann, B. and Schilling, T. F. (1995). Stages of embryonic development of the zebrafish. *Dev. Dyn.* **203**, 253–310.
- Korb, O., Stützle, T. and Exner, T. E. (2007). An ant colony optimization approach to flexible protein–ligand docking. *Swarm Intell.* **1**, 115–134.
- Korb, O., Stützle, T. and Exner, T. E. (2009). Empirical scoring functions for advanced Protein-Ligand docking with PLANTS. *J. Chem. Inf. Model.* **49**, 84–96.
- Koul, A., Arnout, E., Lounis, N., Guillemont, J. and Andries, K. (2011). The challenge of new drug discovery for tuberculosis. *Nature* **469**, 483–490.
- Lakshminarayana, S. B., Huat, T. B., Ho, P. C., Manjunatha, U. H., Dartois, V., Dick, T. and Rao, S. P. S. (2015). Comprehensive physicochemical, pharmacokinetic and activity profiling of anti-TB agents. *J. Antimicrob. Chemother.* **70**, 857–867.
- Lesley, R. and Ramakrishnan, L. (2008). Insights into early mycobacterial pathogenesis from the zebrafish. *Curr. Opin. Microbiol.* **11**, 277–283.
- Ling, J., Reynolds, N. and Ibba, M. (2009). Aminoacyl-tRNA synthesis and translational quality control. *Annu. Rev. Microbiol.* **63**, 61–78.
- Maddry, J. A., Ananthan, S., Goldman, R. C., Hobrath, J. V., Kwong, C. D., Maddox, C., Rasmussen, L., Reynolds, R. C., Secrist, J. A., Sosa, M. I., et al. (2009). Antituberculosis activity of the molecular libraries screening center network library. *Tuberculosis* **89**, 354–363.
- Makarov, V., Lechartier, B., Zhang, M., Neres, J., van der Sar, A. M., Raadsen, S. A., Hartkoorn, R. C., Ryabova, O. B., Vocat, A., Decosterd, L. A., et al. (2014). Towards a new combination therapy for tuberculosis with next generation benzothiazinones. *EMBO Mol. Med.* **6**, 372–383.
- Mase, S. R. and Chorba, T. (2019). Treatment of Drug-Resistant Tuberculosis. *Clin. Chest Med.* **40**, 775–795.

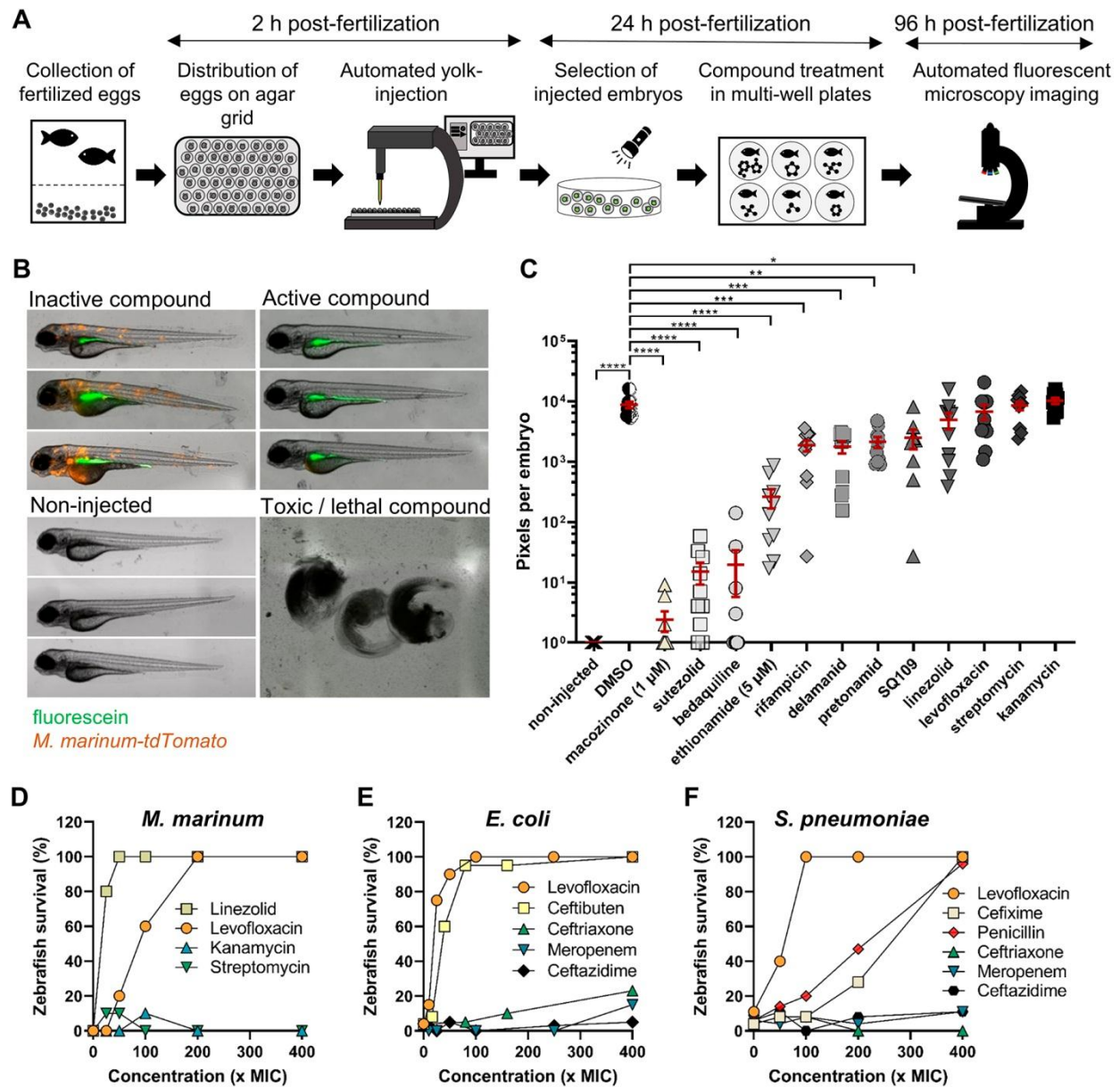
- Meijer, A. H., Verbeek, F. J., Salas-Vidal, E., Corredor-Adámez, M., Bussman, J., van der Sar, A. M., Otto, G. W., Geisler, R. and Spaink, H. P.** (2005). Transcriptome profiling of adult zebrafish at the late stage of chronic tuberculosis due to *Mycobacterium marinum* infection. *Mol. Immunol.* **42**, 1185–1203.
- Morgan, P., Van Der Graaf, P. H., Arrowsmith, J., Feltner, D. E., Drummond, K. S., Wegner, C. D. and Street, S. D. A.** (2012). Can the flow of medicines be improved? Fundamental pharmacokinetic and pharmacological principles toward improving Phase II survival. *Drug Discov. Today* **17**, 419–424.
- Morikane, D., Zang, L. and Nishimura, N.** (2020). Evaluation of the Percutaneous Absorption of Drug Molecules in Zebrafish. *Molecules* **25**.
- Mukhopadhyay, A. and Peterson, R. T.** (2006). Fishing for new antimicrobials. *Curr. Opin. Chem. Biol.* **10**, 327–333.
- Mve-Obiang, A., Mestdagh, M. and Portaels, F.** (2001). DNA isolation from chloroform/methanol-treated mycobacterial cells without lysozyme and proteinase K. *Biotechniques* **30**, 272–276.
- Ollinger, J., Kumar, A., Roberts, D. M., Bailey, M. A., Casey, A. and Parish, T.** (2019). A high-throughput whole cell screen to identify inhibitors of *Mycobacterium tuberculosis*. *PLoS One* **14**, e0205479.
- Ordas, A., Raterink, R. J., Cunningham, F., Jansen, H. J., Wiweger, M. I., Jong-Raadsen, S., Bos, S., Bates, R. H., Barros, D., Meijer, A. H., et al.** (2015). Testing tuberculosis drug efficacy in a zebrafish high-throughput translational medicine screen. *Antimicrob. Agents Chemother.* **59**, 753–762.
- Palomino, J.-C., Martin, A., Camacho, M., Guerra, H., Swings, J. and Portaels, F.** (2002). Resazurin microtiter assay plate: simple and inexpensive method for detection of drug resistance in *Mycobacterium tuberculosis*. *Antimicrob. Agents Chemother.* **46**, 2720–2.
- Paravisi, S., Fumagalli, G., Riva, M., Morandi, P., Morosi, R., Konarev, P. V., Petoukhov, M. V., Bernier, S., Chênevert, R., Svergun, D. I., et al.** (2009). Kinetic and mechanistic characterization of *Mycobacterium tuberculosis* glutamyl-tRNA synthetase and determination of its oligomeric structure in solution. *FEBS J.* **276**, 1398–1417.
- Pethe, K., Sequeira, P. C., Agarwalla, S., Rhee, K., Kuhen, K., Phong, W. Y., Patel, V., Beer, D., Walker, J. R., Duraiswamy, J., et al.** (2010). A chemical genetic screen in *Mycobacterium tuberculosis* identifies carbon-source-dependent growth inhibitors devoid of in vivo efficacy. *Nat. Commun.* **1**, 1–8.
- Pethe, K., Bifani, P., Jang, J., Kang, S., Park, S., Ahn, S., Jiricek, J., Jung, J., Jeon, H. K., Cechetto, J., et al.** (2013). Discovery of Q203, a potent clinical candidate for the treatment of tuberculosis. *Nat. Med.* **19**, 1157–1160.
- Prouty, M. G., Correa, N. E., Barker, L. P., Jagadeeswaran, P. and Klose, K. E.** (2003). Zebrafish-*Mycobacterium marinum* model for mycobacterial pathogenesis. *FEMS Microbiol. Lett.* **225**, 177–182.
- Scherman, M. S., North, E. J., Jones, V., Hess, T. N., Grzegorzewicz, A. E., Kasagami, T., Kim, I. H., Merzlikin, O., Lenaerts, A. J., Lee, R. E., et al.** (2012). Screening a library of 1600 adamantyl ureas for anti-*Mycobacterium tuberculosis* activity in vitro and for better physical chemical properties for bioavailability. *Bioorganic Med. Chem.* **20**, 3255–3262.
- Schulthess, P., Van Wijk, R. C., Krekels, E. H. J., Yates, J. W. T., Spaink, H. P. and Van Der Graaf, P. H.** (2018). Outside-in systems pharmacology combines innovative computational methods with high-throughput whole vertebrate studies. *CPT Pharmacometrics Syst. Pharmacol.* **7**, 285–287.

- Seung, K. J. and Hewison, C.** (2019). Now is the time for shorter all-oral regimens for multidrug-resistant tuberculosis. *Lancet Glob. Heal.* **7**,.
- Singh, A. K. and Gupta, U. D.** (2018). Animal models of tuberculosis: Lesson learnt. *Indian J. Med. Res.* **147**, 456–463.
- Soto, R., Perez-Herran, E., Rodriguez, B., Duma, B. M., Cacho-Izquierdo, M., Mendoza-Losana, A., Lelievre, J., Aguirre, D. B., Ballell, L., Cox, L. R., et al.** (2018). Identification and characterization of aspartyl-tRNA synthetase inhibitors against *Mycobacterium tuberculosis* by an integrated whole-cell target-based approach. *Sci. Rep.* **8**, 12664.
- Spaink, H. P., Cui, C., Wiweger, M. I., Jansen, H. J., Veneman, W. J., Marín-Juez, R., de Sonnevile, J., Ordas, A., Torraca, V., van der Ent, W., et al.** (2013). Robotic injection of zebrafish embryos for high-throughput screening in disease models. *Methods* **62**, 246–254.
- Stanley, S. A., Grant, S. S., Kawate, T., Iwase, N., Shimizu, M., Wivagg, C., Silvis, M., Kazyanskaya, E., Aquadro, J., Golas, A., et al.** (2012). Identification of novel inhibitors of *M. tuberculosis* growth using whole cell based high-throughput screening. *ACS Chem. Biol.* **7**, 1377–1384.
- Stoop, E. J. M. M., Schipper, T., Rosendahl Huber, S. K., Nezhinsky, A. E., Verbeek, F. J., Gurcha, S. S., Besra, G. S., Vandenbroucke-Grauls, C. M. J. E. J. E., Bitter, W. and Van Der Sar, A. M.** (2011). Zebrafish embryo screen for mycobacterial genes involved in the initiation of granuloma formation reveals a newly identified ESX-1 component. *Dis. Model. Mech.* **4**, 526–536.
- Stop TB Partnership** (2019). The Paradigm Shift: Global Plan to End TB: 2018-2022.
- Takaki, K., Cosma, C. L., Troll, M. A. and Ramakrishnan, L.** (2012). An in vivo platform for rapid high-throughput antitubercular drug discovery. *Cell Rep.* **2**, 175–184.
- Tobin, D. M. and Ramakrishnan, L.** (2008). *Comparative pathogenesis of Mycobacterium marinum and Mycobacterium tuberculosis*. *Cell Microbiol.*
- van Buuren, S. and Groothuis-Oudshoorn, K.** (2011). mice: Multivariate imputation by chained equations in R. *J. Stat. Softw.* **45**, 1–67.
- Van Der Sar, A. M., Abdallah, A. M., Sparrius, M., Reinders, E., Vandenbroucke-Grauls, C. M. J. E. and Bitter, W.** (2004). *Mycobacterium marinum* strains can be divided into two distinct types based on genetic diversity and virulence. *Infect. Immun.* **72**, 6306–6312.
- Van Der Vaart, M., Spaink, H. P. and Meijer, A. H.** (2012). Pathogen recognition and activation of the innate immune response in zebrafish. *Adv. Hematol.* **2012**,.
- van Wijk, R. C., Krekels, E. H. J., Kantae, V., Harms, A. C., Hankemeier, T., van der Graaf, P. H. and Spaink, H. P.** (2019). Impact of post-hatching maturation on the pharmacokinetics of paracetamol in zebrafish larvae. *Sci. Rep.* **9**, 1–9.
- van Wijk, R. C., Ayoun Alsoud, R., Lennernäs, H. and Simonsson, U. S. H.** (2020a). Model-Informed Drug Discovery and Development Strategy for the Rapid Development of Anti-Tuberculosis Drug Combinations. *Appl. Sci.* **10**, 2376.
- van Wijk, R. C., Hu, W., Dijkema, S. M., van den Berg, D. J., Liu, J., Bahi, R., Verbeek, F. J., Simonsson, U. S. H., Spaink, H. P., van der Graaf, P. H., et al.** (2020b). Anti-tuberculosis effect of isoniazid scales accurately from zebrafish to humans. *Br. J. Pharmacol.* **177**, 5518–5533.



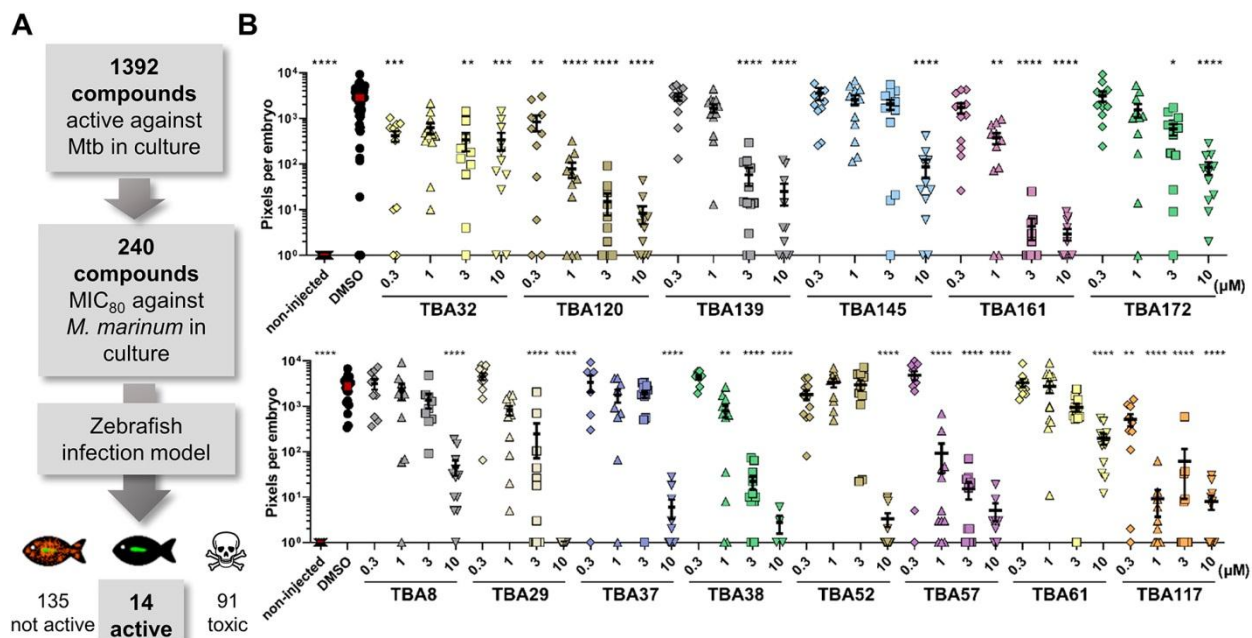
- Van Wijk, R. C., Krekels, E. H. J., Kantae, V., Ordas, A., Kreling, T., Harms, A. C., Hankemeier, T., Spaink, H. P. and Van Der Graaf, P. H.** (2019). Mechanistic and quantitative understanding of pharmacokinetics in zebrafish larvae through nanoscale blood sampling and metabolite modeling of paracetamol. *J. Pharmacol. Exp. Ther.* **371**, 15–24.
- Veneman, W. J., Marín-Juez, R., de Sonnevile, J., Ordas, A., Jong-Raadsen, S., Meijer, A. H., Spaink, H. P. and Sonnevile, D.** (2014). Establishment and Optimization of a High Throughput Setup to Study *Staphylococcus epidermidis* and *Mycobacterium marinum* Infection as a Model for Drug Discovery. *J. Vis. Exp* **88**, 51649.
- Walter, F., Pütz, J., Giegé, R. and Westhof, E.** (2002). Binding of tobramycin leads to conformational changes in yeast tRNA<sup>Asp</sup> and inhibition of aminoacylation. *EMBO J.* **21**, 760–768.
- Wang, W., Liu, X., Gelinas, D., Ciruna, B. and Sun, Y.** (2007). A Fully Automated Robotic System for Microinjection of Zebrafish Embryos. *PLoS One* **2**, e862.
- Weerdenburg, E. M., Abdallah, A. M., Rangkuti, F., El Ghany, M. A., Otto, T. D., Adroub, S. A., Molenaar, D., Ummels, R., ter Veen, K., van Stempvoort, G., et al.** (2015). Genome-wide transposon mutagenesis indicates that *Mycobacterium marinum* customizes its virulence mechanisms for survival and replication in different hosts. *Infect. Immun.* **83**, 1778–1788.
- White, R. M., Sessa, A., Burke, C., Bowman, T., LeBlanc, J., Ceol, C., Bourque, C., Dovey, M., Goessling, W., Burns, C. E., et al.** (2008). Transparent Adult Zebrafish as a Tool for In Vivo Transplantation Analysis. *Cell Stem Cell* **2**, 183–189.
- WHO** (2020a). Global tuberculosis report 2020.
- WHO** (2020b). *WHO consolidated guidelines on tuberculosis Module 4: Treatment Drug-resistant tuberculosis treatment.*
- Wicha, S. G., Clewe, O., Svensson, R. J., Gillespie, S. H., Hu, Y., Coates, A. R. M. and Simonsson, U. S. H.** (2018). Forecasting Clinical Dose–Response From Preclinical Studies in Tuberculosis Research: Translational Predictions With Rifampicin. *Clin. Pharmacol. Ther.* **104**, 1208–1218.
- Woese, C. R., Olsen, G. J., Ibba, M. and Söll, D.** (2000). Aminoacyl-tRNA Synthetases, the Genetic Code, and the Evolutionary Process. *Microbiol. Mol. Biol. Rev.* **64**, 202–236.

## Figures

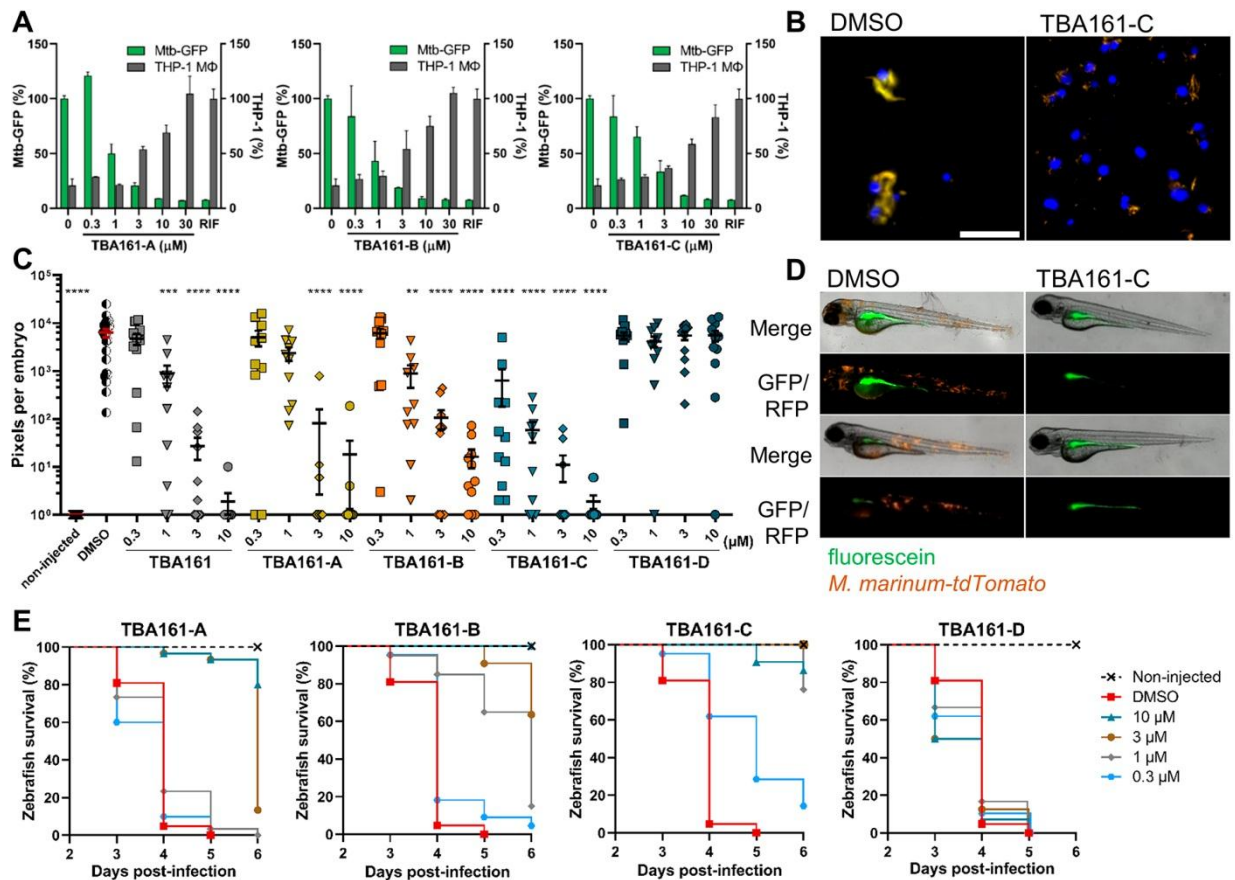


**Fig. 1. Zebrafish embryo infection model can be used for medium-throughput compound screening and can predict oral bioavailability of test compounds (A)** Schematic representation of the *in vivo* drug-screening set-up in the zebrafish-*M. marinum* infection model. **(B)** Representative images of different read-out groups of *M. marinum* infected zebrafish embryos. **(C)** *M. marinum-tdTomato* yolk-infected zebrafish embryos treated with antibiotics at 10  $\mu$ M, or as specified. Each data point represents the integrated red-fluorescence intensity of a single zebrafish embryo, and the signal of each group (10-12 embryos) is expressed as mean  $\pm$  SEM. Data analysis was performed as described in the methods section. Significance is indicated as: \*  $p \leq 0.05$ ; \*\*  $p \leq 0.01$ ; \*\*\*  $p \leq 0.001$ ; \*\*\*\*  $p \leq 0.0001$  **(D)** Zebrafish embryos were yolk-infected with *M. marinum-tdTomato* and at 24 hpi treated by adding the antibiotics into the fish water. Survival was scored 4 dpi. Each group consisted of 10 embryos. Non-treated group of embryos (0

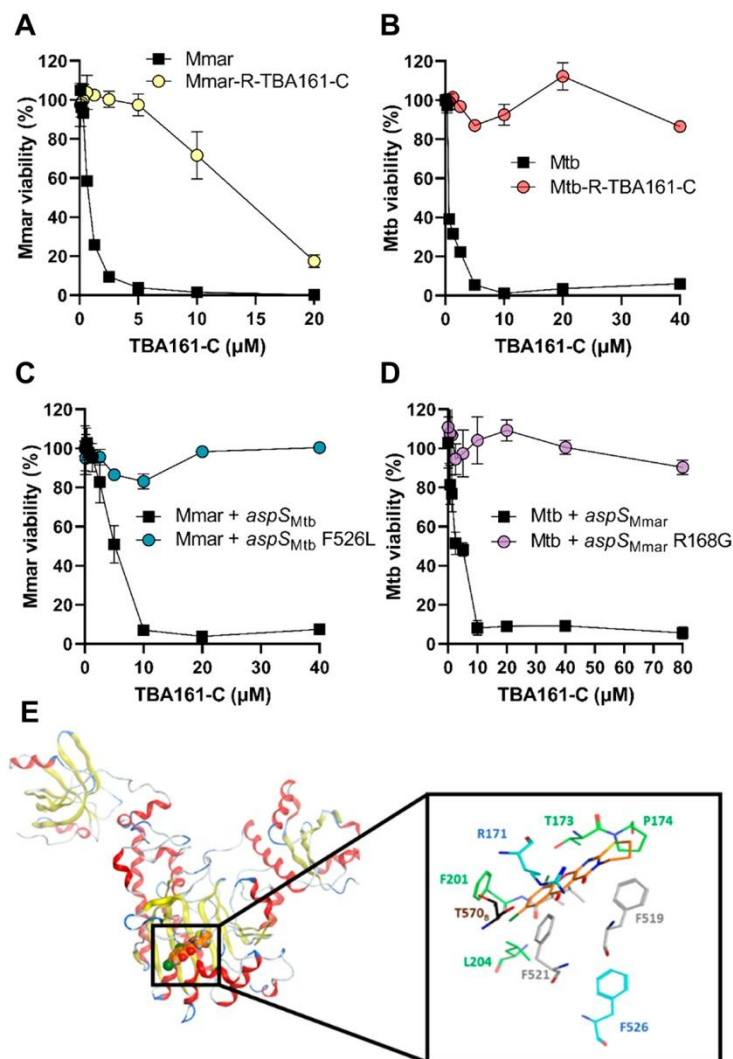
x MIC) served as control. **(E)** Zebrafish were infected via the caudal vein route with *E. coli* GK1161434 or **(F)** *S. pneumonia* D39V and 1 hpi treated by addition of the antibiotics to the fish water. Survival was scored 24 hpt. Each group consisted of 20-40 embryos. Concentrations of all antibiotics were based on the antibiotic's minimal inhibitory concentration (MIC) value for each strain, see Table S1. Non-treated group of embryos (0 x MIC) served as control.



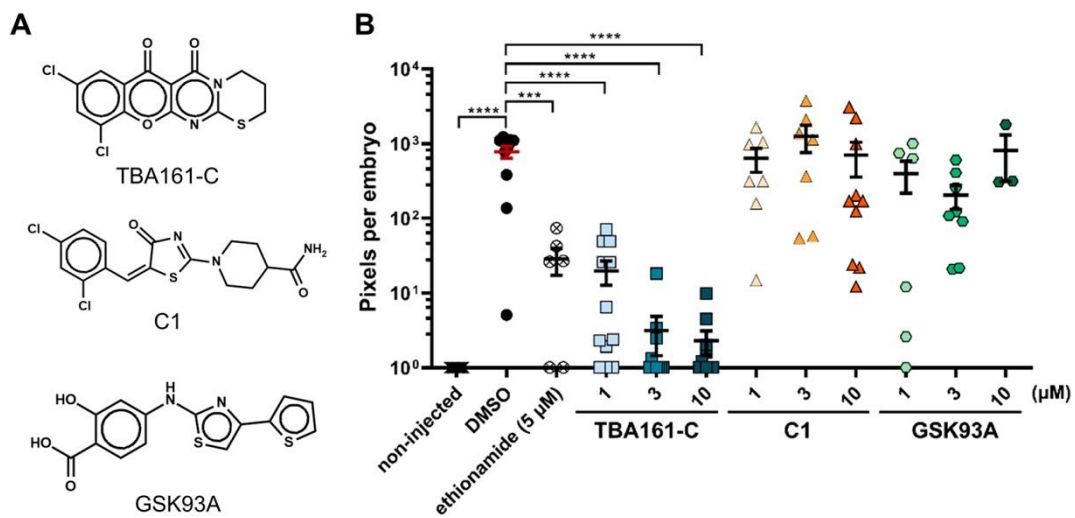
**Fig. 2. Screening a library of anti-mycobacterial compounds in zebrafish-infection model identifies 14 hit-compounds. (A)** Scheme of screen design: Compounds active against Mtb and *M. marinum* *in vitro* were tested in the zebrafish embryo-*M. marinum* yolk-infection model. **(B)** Hit compounds were tested in a dose-response assay. Each data point represents the integrated red-fluorescence intensity of a single zebrafish embryo, and the signal of each group (10-20 embryos) is expressed as mean  $\pm$  SEM. Data analysis was performed as described in the methods section. Significance was calculated by comparing each treatment group with DMSO treated control group and is indicated as: \*  $p \leq 0.05$ ; \*\*  $p \leq 0.01$ ; \*\*\*  $p \leq 0.001$ ; \*\*\*\*  $p \leq 0.0001$ .



**Fig. 3. Activity of TBA161 variants in macrophage and zebrafish infection models.** (A) THP-1 macrophages were infected with Mtb carrying pTetDuo, expressing *gfp* under tetracycline-inducible promoter and *tdTomato* under the constitutive promoter  $P_{myc}$ . Infected macrophages were treated with various doses of each test compound for 6 days. The *gfp* expression was induced by the addition of ATc and macrophage nuclei were stained with Hoechst dye to detect macrophages (grey bars). The GFP signal within each macrophage was quantified, representing the amount of viable bacteria (green bars). DMSO and rifampicin (RIF, 3μM) treated samples served as a negative and positive control, respectively. Data points represent the average of duplicates with the standard deviations. (B) Representative images of Mtb-pTetDuo infected THP-1 macrophages treated with DMSO or compound TBA161-C at 6 dpt. Blue: macrophage nuclei (Hoechst); red and green: Mtb expressing *tdTomato* and *gfp*. Scale bar represents 50 μM. (C) Dose-dependent activity of TBA161 variants in the zebrafish-*M. marinum* infection model. Each data point represents the integrated red-fluorescence intensity of a single zebrafish embryo, and the signal of each group (10-20 embryos) is expressed as mean ± SEM. Data analysis was performed as described in the methods section. Significance was calculated by comparing each treatment group with DMSO treated group and is indicated as: \*  $p \leq 0.05$ ; \*\*  $p \leq 0.01$ ; \*\*\*  $p \leq 0.001$ ; \*\*\*\*  $p \leq 0.0001$ . (D) Representative images of *M. marinum*-*tdTomato*-yolk-infected zebrafish embryos treated with DMSO (left) or TBA161-C (right) on 3 dpt. (E) Survival curves of *M. marinum* yolk-infected zebrafish embryos after dose-dependent drug treatment. The treatment started at 1 day post-infection by adding compounds to the fish water. Each treatment group consisted of 25-30 embryos.



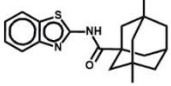
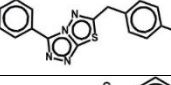
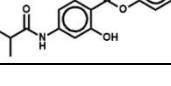
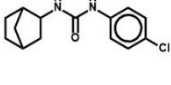
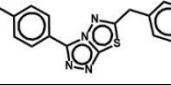
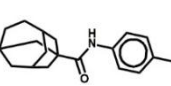
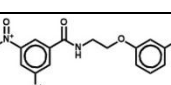
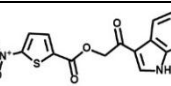
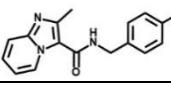
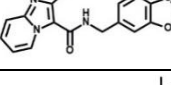
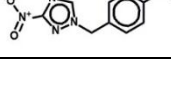
**Fig. 4. Mutations in *aspS* are associated with TBA161-C resistance.** (A) Susceptibility of *M. marinum* WT (Mmar) and TBA161-C resistant isolates (Mmar-R-TBA161-C) towards TBA161-C after 4 days of incubation. Data is presented as mean of duplicates  $\pm$  SD. (B) Susceptibility of Mtb WT and TBA-161 resistant isolates (Mtb-R-TBA161-C) towards TBA161-C was measured after 7 days. Data is presented as mean of duplicates  $\pm$  SD. (C) *M. marinum* WT transformed with pMS2-*aspS<sub>Mtb</sub>* (Mmar+*aspS<sub>Mtb</sub>*), pMS2-*aspS<sub>Mtb</sub>*F526L (Mmar+*aspS<sub>Mtb</sub>*F526L) were incubated with compound TBA161-C for 4 days at indicated concentrations. (D) Mtb carrying plasmids pMS2-*aspS<sub>Mmar</sub>* (Mtb+*aspS<sub>Mmar</sub>*), pMS2-*aspS<sub>Mmar</sub>*R168G (Mtb+*aspS<sub>Mmar</sub>*R168G) were incubated with 2-fold dilutions of compound TBA161-C for 7 days. Data is presented as mean of duplicates  $\pm$  SD. (E) TBA161-C (orange) docked into the catalytic subdomain of chain A of Mtb AspS (PDB ID: 5W25 (Dranow, D.M., Lorimer, D.D., Edwards, 2017)). The zoom-in shows TBA161-C in stick representation, together with AspS residues aligning the binding pocket. These include R171 (blue), the three residues of which side chains were treated flexible during docking (grey), and T570 of chain B (dark brown). The distant F526 residue is shown in blue as well. For clarity, the L200 label and all hydrogen atoms are omitted.



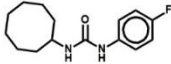
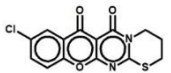
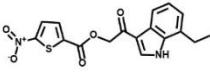
**Fig. 5. TBA161-C has a potent activity in the zebrafish infection model as compared to other AspS inhibitors.** (A) The chemical structures of the test compounds. (B) Zebrafish embryos were yolk-injected with *M. marinum*-*tdTomato* and treated with compounds at indicated concentrations. Each data point represents the integrated red-fluorescence intensity of a single zebrafish embryo, and the signal of each group is expressed as mean  $\pm$  SEM. Data analysis was performed as described in the methods section. Significance is indicated as: \*\*\* $p \leq 0.001$ ; \*\*\*\* $p \leq 0.0001$

## Tables

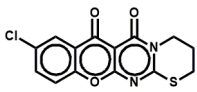
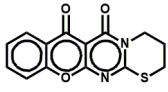
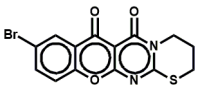
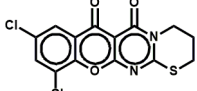
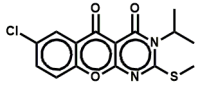
**Table 1. Activity and characteristics of TBA hit-compounds that show activity in the zebrafish-*M. marinum* infection model.** The *in vitro* activity represents compounds' activity against growing bacteria in culture. The *ex-vivo* activity represents compounds intracellular activity in *M.tuberculosis*-infected THP-1 macrophages. MIC<sub>90</sub> and MIC<sub>50</sub> represent the minimal inhibitory concentration required to inhibit 90% or 50% of bacterial growth, respectively. The MIC values were determined by generating dose-response curves using a nonlinear fitting of the data with a variable slope. Data is presented as mean ± SD. (Mmar: *M. marinum* M<sup>USA</sup>; Mtb: *M. tuberculosis* H37Rv; MoA: mechanism of action).

Compound ID	Structure	MIC <sub>90</sub> Mtb <i>in vitro</i> (μM)	MIC <sub>50</sub> Mtb <i>ex-vivo</i> (μM)	Proposed target / MoA
TBA8		15.8 ± 7.5	6.9 ± 8.7	MmpL3 (Graham et al., 2018)
TBA29		3.6 ± 0.9	6.1 ± 4.0	Cytochrome bc1 (Arora et al., 2014)
TBA32		2.0 ± 0.5	9.6 ± 16.6	Thymidylate synthase (Hearn et al., 2014)
TBA37		13.6 ± 4.3	5.5 ± 3.6	MmpL3 (Brown et al., 2011; Grzegorzewicz et al., 2012b; Scherman et al., 2012)
TBA38		9.9 ± 1.9	5.6 ± 3.4	Cytochrome bc1 (Arora et al., 2014)
TBA52		9.6 ± 5.3	4.2 ± 6.0	MmpL3 (Brown et al., 2011; Grzegorzewicz et al., 2012b; Scherman et al., 2012)
TBA57		1.7 ± 3.1	1.6 ± 0.7	DprE1 (Christophe et al., 2009b)
TBA61		2.2 ± 0.2	> 30	Inhibitor of folate biosynthesis (Johnson et al., 2019)
TBA117		4.0 ± 1.4	0.4 ± 0.1	Cytochrome bc1 (Pethe et al., 2013)
TBA120		5.9 ± 2.6	0.5 ± 0.2	Cytochrome bc1 (Pethe et al., 2013)
TBA139		11.8 ± 12.4	4.6 ± 7.1	DprE1 (Stanley et al., 2012)



TBA145		$19.0 \pm 5.7$	$8 \pm 14.2$	MmpL3 (Brown et al., 2011; Grzegorzewicz et al., 2012b; Scherman et al., 2012)
TBA161		$14.6 \pm 7.3$	$2.5 \pm 1.0$	Unknown
TBA172		$2.4 \pm 0.4$	> 30	Inhibitor of folate biosynthesis (Johnson et al., 2019)

**Table 2. Structures and activity of TBA161 variants.** The *in vitro* activity represents compounds' activity against growing bacteria in culture. The *ex-vivo* activity represents compounds' intracellular activity in *M.tuberculosis*-infected THP-1 macrophages. MIC<sub>90</sub> and MIC<sub>50</sub> represent the minimal inhibitory concentration required to inhibit 90% or 50% of bacterial growth, respectively. The MIC values were determined by generating dose-response curves using a nonlinear fitting of the data with a variable slope. Data is presented as mean ± SD. (Mmar: *M. marinum* M<sup>USA</sup>; Mtb: *M. tuberculosis* H37Rv).

Compound ID	Structure	MIC <sub>90</sub> Mmar <i>in vitro</i> (μM)	MIC <sub>90</sub> Mtb <i>in vitro</i> (μM)	MIC <sub>50</sub> Mtb <i>ex-vivo</i> (μM)
TBA161		3.1 ± 0.6	14.6 ± 7.3	2.5 ± 1.0
TBA161-A		2.8 ± 1.7	3.8 ± 3.1	1.1 ± 0.9
TBA161-B		2.2 ± 0.2	3.6 ± 2.2	0.9 ± 0.6
TBA 161-C		1.3 ± 0.1	1.3 ± 0.7	1.7 ± 0.7
TBA161-D		> 20	> 20	> 30

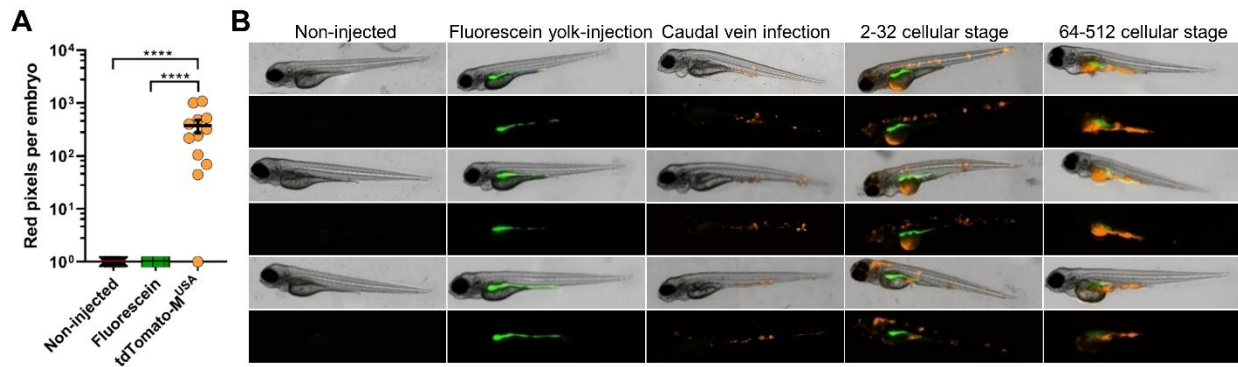


**Fig. S1. Bacterial localization within infected zebrafish depends on the time-point of infection.** **(A)** Zebrafish embryos were yolk-infected with fluorescein or *M. marinum* expressing *tdTomato* mixed with fluorescein. At 4 dpi the red-fluorescence intensity was quantified after imaging and used as a readout. Each data point represents the integrated red-fluorescence intensity of a single zebrafish embryo and the signal of each group is expressed as mean  $\pm$  SEM. Data analysis was performed as described in the methods section. Significance is indicated as: \*\*\*\*  $p \leq 0.0001$ . **(B)** Representative fluorescence images of embryos infected via caudal vein at 1 dpf or infected via yolk injections at 2-32 or 64-512 cellular stages. Four days after injection, fluorescence images were generated. The green-fluorescent dye fluorescein served as an injection control and the red-fluorescent signal corresponds to the bacterial load of *M. marinum*.

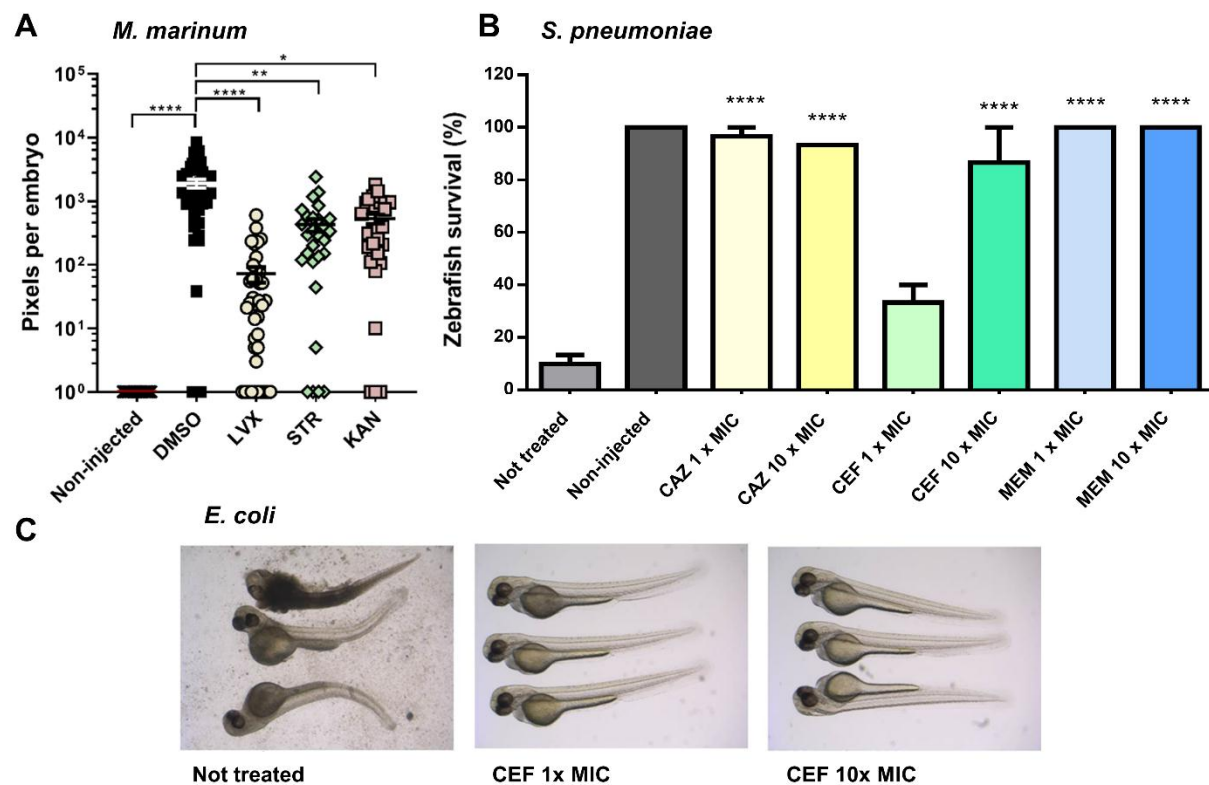


**Fig. S2. Treatment of infected zebrafish by intravenous drug injection is effective for antibiotics that are administered intravenously. (A)** Zebrafish embryos were 1 dpf intravenously infected with *M. marinum*-tdTomato and 24h later treated by intravenous injection of indicated antibiotics. On 4 dpi fluorescence images were generated and the integrated red-fluorescence intensity was quantified. Each data point represents the integrated red-fluorescence intensity of a single zebrafish embryo and the signal of each group is expressed as mean  $\pm$  SEM. Data analysis was performed as described in the methods section. Significance is indicated as: \*  $p \leq 0.05$ ; \*\*  $p \leq 0.01$ ; \*\*\*  $p \leq 0.001$ ; \*\*\*\*  $p \leq 0.0001$ . **(B)** Zebrafish embryos were 1 dpf intravenously infected with *S. pneumoniae* D39V and 1 hpi treated by intravenous injection with 1 or 10 times the MIC value (see Table S1) of ceftazidime (CAZ), ceftriaxone (CEF), or meropenem (MEM). Infected zebrafish with no treatment and non-infected zebrafish served as negative and positive control, respectively. The zebrafish survival was scored 24 hpt. The significant difference in comparison to the negative control group is indicated as: \*  $p \leq 0.05$ ; \*\*  $p \leq 0.01$ ; \*\*\*  $p \leq 0.001$ ; \*\*\*\*  $p \leq 0.0001$ . **(C)** Zebrafish embryos that were 1 dpf

intravenously infected with *E.coli* GSK1161343 and 1 hpf treated by intravenous injection with 1 or 10 times the MIC value (see Table S1) of ceftriaxone (CEF). The control group consisted of non-infected and non-treated zebrafish. The zebrafish survival was scored 24 hpt and is presented as a representative image of each treatment group.

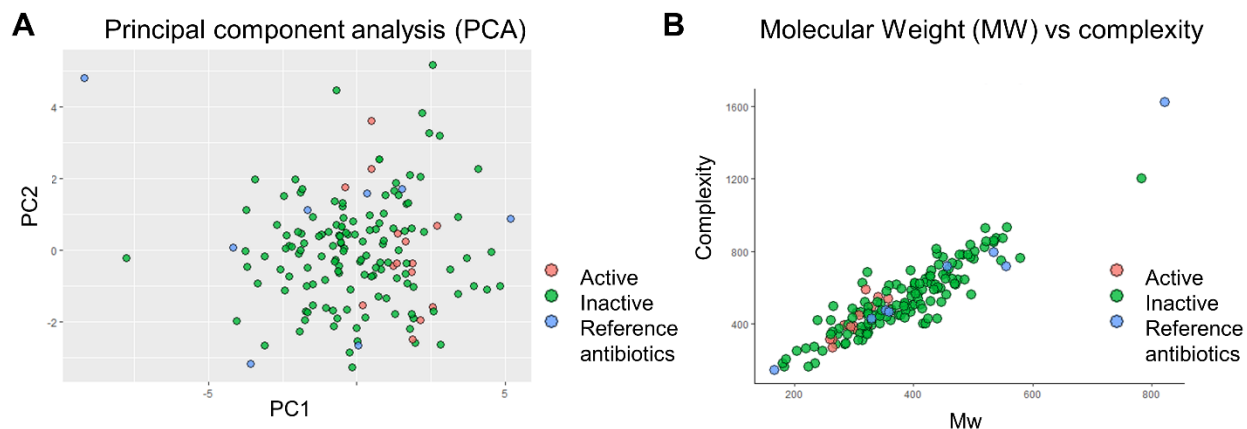


**Fig. S3. Compounds activity in the zebrafish infection model cannot be predicted on compounds physicochemical properties. (A)** Visual representation of performed principal component analysis (PCA). Compounds were divided into three activity classes, based on their activity in the zebrafish-infection model: active compounds (14), inactive compounds (135), active reference antibiotics (macozinone, sutezolid, bedaquiline, ethionamide, rifampicin, delamanid, SQ109, pretonamid). **(B)** Graph comparing the molecular weight (MW) and complexity of each compound of the three activity classes. Complexity value is based on the elements and structural features of the molecule (Bertz, 2002; Hendrickson et al., 1987).

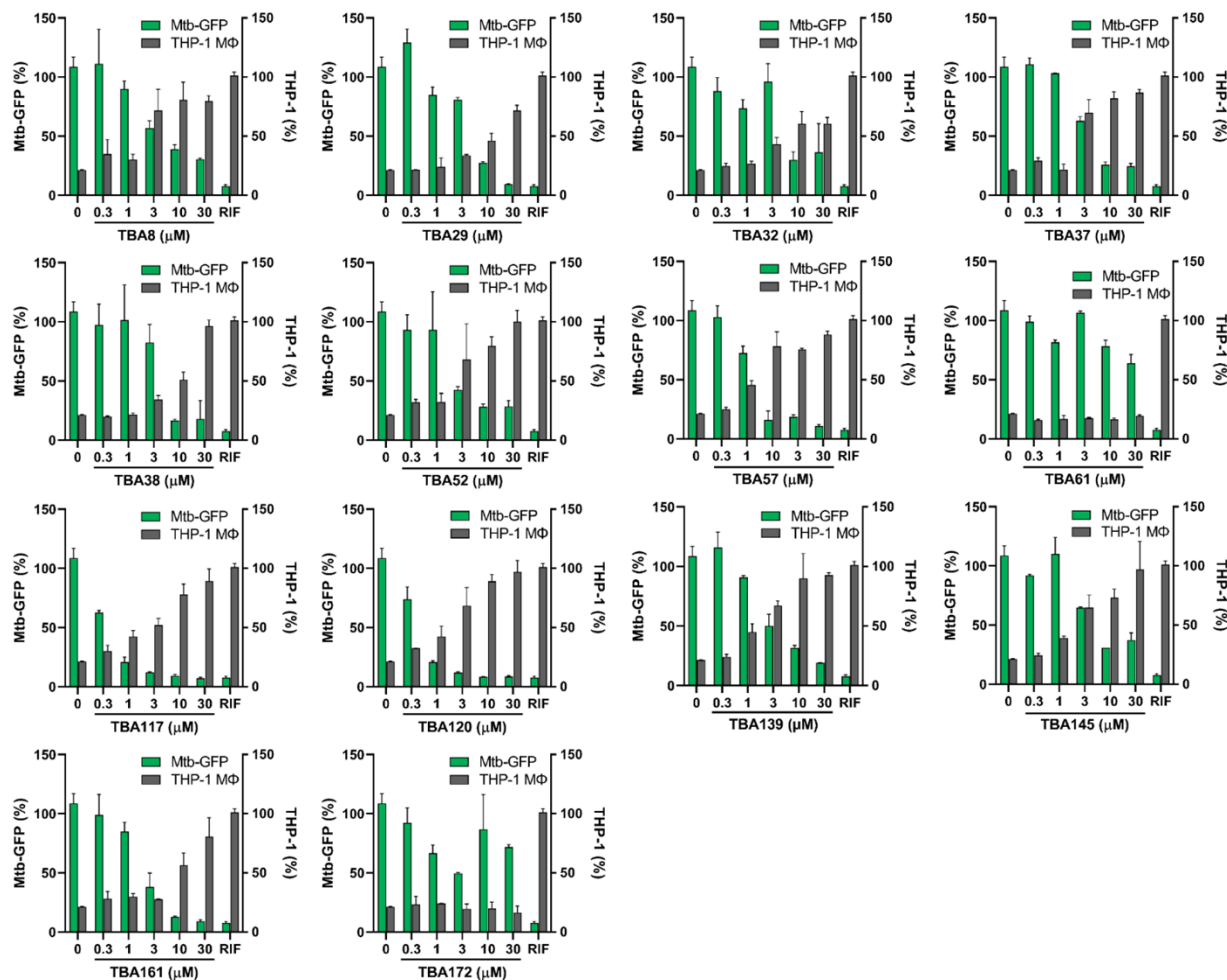


**Fig. S4. Activity of TBA hit-compounds in the macrophage infection model.** TBA hit compounds from zebrafish-infection model were tested for their intracellular activity in infected macrophages. THP-1 macrophages were infected with Mtb carrying pTetDuo, expressing *gfp* under control of a ATc -inducible promoter and *tdTomato* under the constitutive promoter. Infected macrophages were treated with various concentrations of each test compound for 5 days. The *gfp* expression was induced by the addition of ATc and macrophage nuclei were stained with Hoechst dye to detect macrophages (grey bars). The GFP signal within each macrophage was quantified, representing the amount of viable bacteria (green bars). DMSO and rifampicin (RIF, 3μM) treated samples served as a negative and positive control, respectively. Data points represent the average of duplicates with the standard deviations.

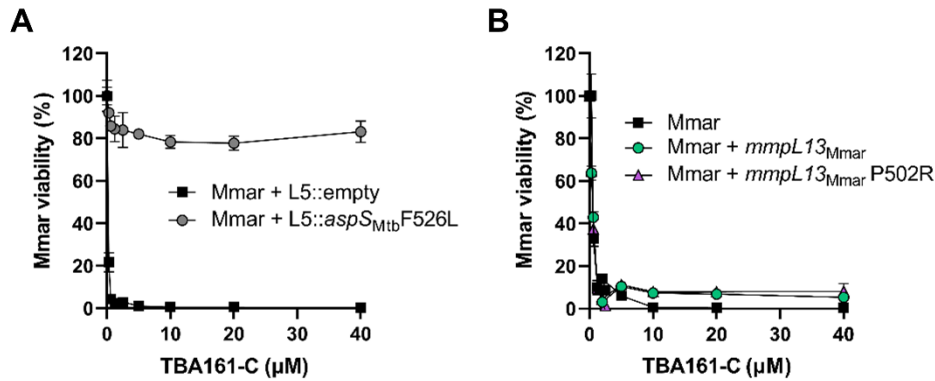


**Fig. S5. Validation of mutations involved in TBA161-C resistance (A)** *M. marinum* WT transformed with empty integrative plasmid pML1342 (Mmar + L5::empty) and *M. marinum* WT transformed with pML1342-*aspS*<sub>Mtb</sub>F526L (Mmar + L5::*aspS*<sub>Mtb</sub>F526L) were incubated with compound TBA161-C for 4 days at indicated concentrations. Data is presented as mean of triplicates  $\pm$  SD. **(B)** Susceptibility of *M. marinum* WT (Mmar) and *M. marinum* WT transformed with pMN016-*mmpL13*<sub>Mmar</sub> (Mmar + *mmpL13*) and pMN016-*mmpL13*<sub>Mmar</sub> P502R (Mmar + *mmpL13* P502R) was measured after 4 days of incubation with TBA161-C. Data is presented as mean of duplicates  $\pm$  SD.



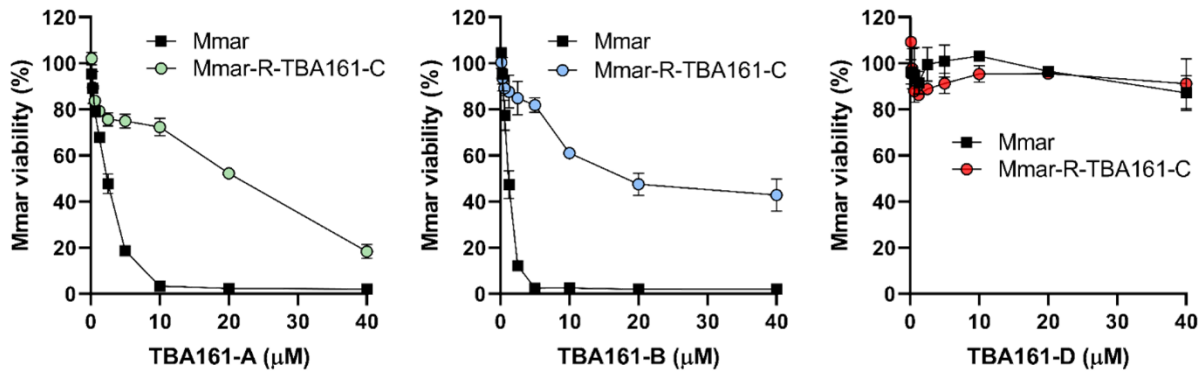


**Fig. S6. TBA161-A and TBA161-B exhibit cross-resistance to TBA161-C resistant *M. marinum* strains.** Susceptibility of *M. marinum* WT strain (Mmar) and TBA161-C resistant isolate (Mmar-R-TBA161-C) after 4 days of incubation with TBA161-A, TBA161-B, TBA161-D. Data is presented as mean of duplicates  $\pm$  SD.

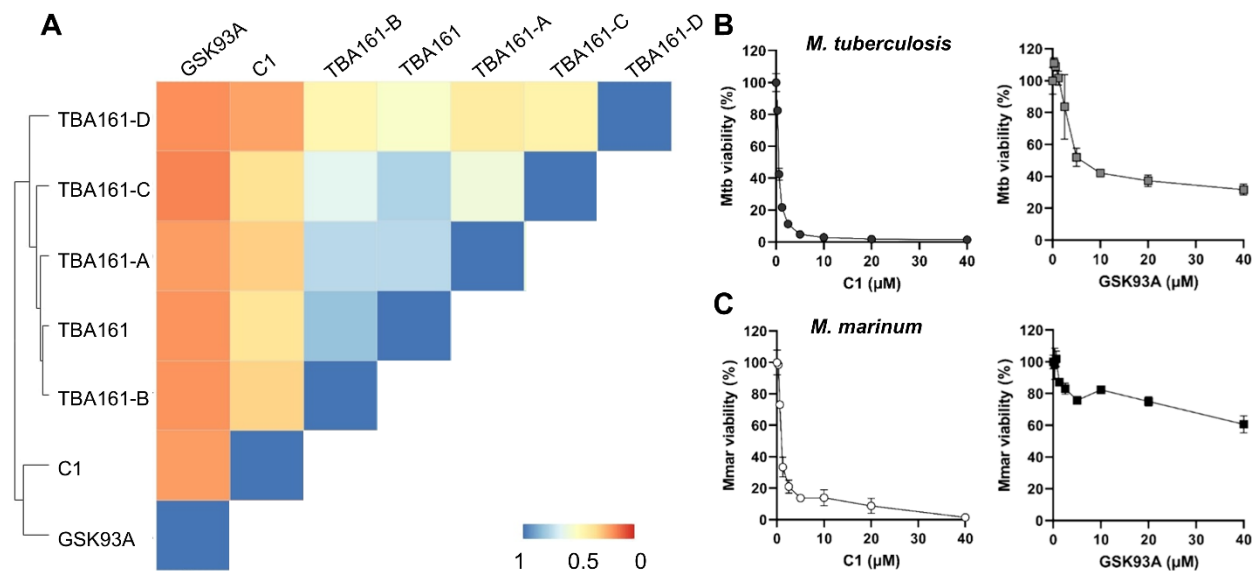


**Fig. S7. Different AspS inhibitors exhibit low structure similarity and dissimilar activity.** **(A)** Tanimoto coefficient graph comparing structure similarities of different TBA variants (TBA161, TBA161-A, TBA161-B, TBA161-C, TBA161-D) and AspS inhibitors (C1, GSK93A), created using ChemMine Tools (Backman et al., 2011). Value 0 describes the lowest similarity, and value 1 describes the highest similarity (identical). **(B)** Susceptibility of *M. marinum* strain towards compounds C1 or GSK93A after 4 days of incubation. Data is presented as mean of duplicates  $\pm$  SD. **(C)** Susceptibility of Mtb WT strain towards compounds C1 or GSK93A after 7 days of incubation. Data is presented as mean of duplicates  $\pm$  SD.

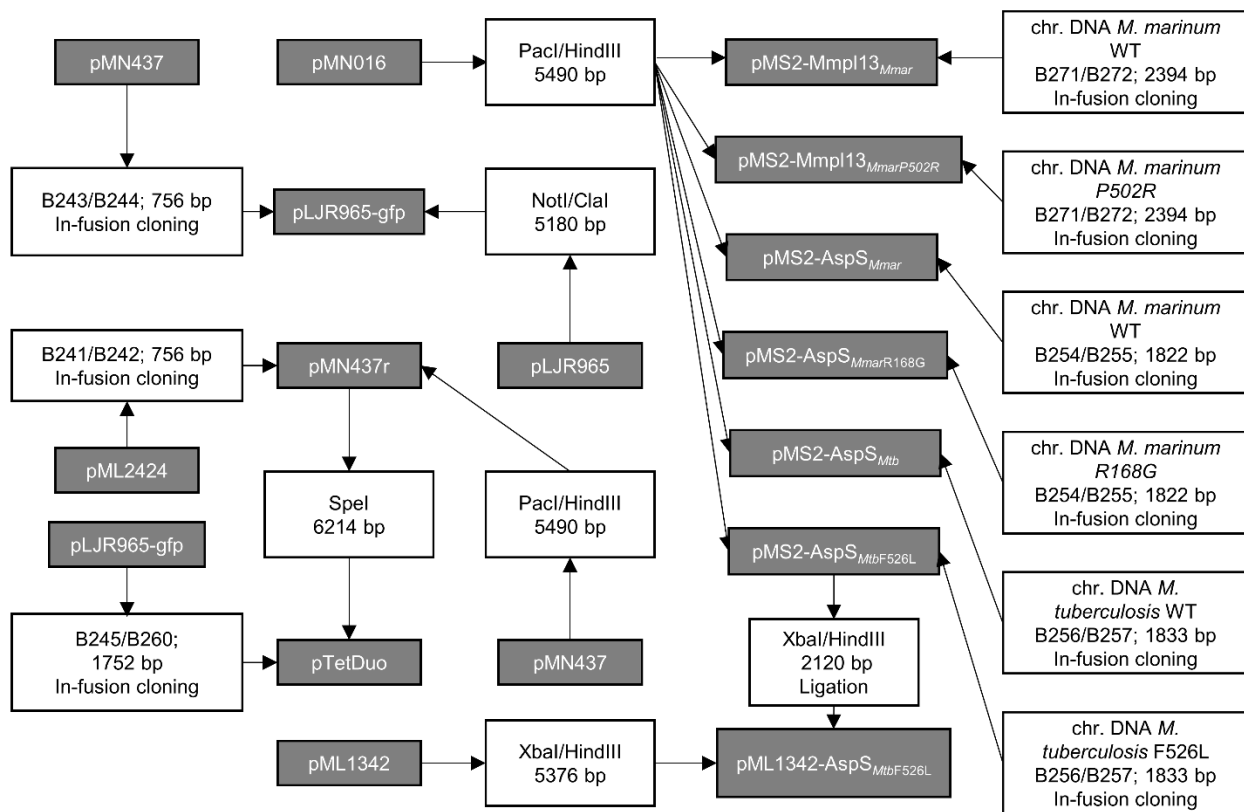


**Fig. S8. Cloning strategy for new plasmids used in this study.** Constructed plasmids are included in grey boxes. The primer pairs used for PCR amplification and correlated restriction enzymes for cloning are listed in white boxes. The DNA template for the PCR reactions is listed above the primer pairs. If several primer pairs are listed, overlap PCR was used to fuse the PCR fragments. When a DNA fragment was obtained by cloning of a plasmid, the utilized restriction enzymes and the length of the obtained fragments are indicated. Constructed primers with their sequences and plasmids with their features and are listed in Tables S5 and S6, respectively.

**Table S1. Minimal inhibitory concentration (MIC) of antibiotics against *M. marinum*, *E. coli* and *S.pneumoniae*.** MIC<sub>90</sub> values represent the concentration required to inhibit 90% of bacterial growth. Not determined: n.d.

Antibiotic	MIC <sub>90</sub> (μM)		
	<i>M. marinum</i>	<i>E. coli</i>	<i>S. pneumoniae</i>
Ceftriaxone	n.d.	0.19	0.05
Ceftazidime	n.d.	n.d.	0.91
Kanamycin	2	n.d.	n.d.
Levofloxacin	1.3	0.35	5.53
Linezolid	4	n.d.	n.d.
Meropenem	n.d.	0.14	0.29
Penicillin	n.d.	n.d.	0.04
Streptomycin	3	n.d.	n.d.

**Table S2. Activity of TBA161-C against selected microorganism, cytotoxicity and zebrafish embryo toxicity.** MIC<sub>90</sub> values represent minimal inhibitory concentration required to inhibit 90% of bacterial growth. TD<sub>50</sub> values represent median toxic dose, a dose required to kill half the members of a tested population.

Organism / cell line	MIC <sub>90</sub> (μM)	TD <sub>50</sub> (μM)
<i>Escherichia coli</i> K12	> 80	
<i>Bacillus subtilis</i> 168	> 80	
<i>Klebsiella pneumoniae</i> LMG20218	> 80	
<i>Acinetobacter baumannii</i> LMG01041	> 80	
<i>Acinetobacter baumannii</i> 1757	> 80	
<i>Mycobacterium abscessus</i> 144C	> 40	
<i>Mycobacterium abscessus</i> RIVM	> 40	
THP-1 cell line		> 40
RAW 264.7 cell line		> 40
<i>Danio rerio</i> embryos		> 40
<i>Danio rerio</i> embryos (1% DMSO)		> 80

**Table S3A.** Single nucleotide polymorphisms identified in TBA161-C resistant *M. marinum*-tdTomato mutants.

Strain	Position	Count/Coverage	Gene mutation	Amino acid change	Gene
R1/R2/R3	5296034	193/194	G-C	P-R (502)	MMAR_4305 ( <i>mmpL13</i> )
R1/R2/R3	25992266	173/174	C-G	R-G (168)	MMAR_2158 ( <i>aspS</i> )

**Table S3B.** Single nucleotide polymorphisms identified in TBA161-C resistant *M. tuberculosis* mutants.

Strain	Position	Count/Coverage	Gene mutation	Amino acid change	Gene
R1	636175	701/702	Deletion (C)	Frameshift	Rv0544c
R1	2896236	705/707	G-C	F-L(526)	Rv2572c ( <i>aspS</i> )
R1	204312	692/711	Deletion (A)	Frameshift	Rv0173 ( <i>lprK</i> )

**Table S4.** Strains used in this study.

Strain	Characteristics	References
<i>Acinetobacter baumannii</i> 1757	Clinical isolate	This study
<i>Acinetobacter baumannii</i> LMG01041	Laboratory strain	(Li et al., 2018)
<i>Bacillus subtilis</i> 168	Laboratory strain	ATCC 23857
<i>Escherichia coli</i> DH5 $\alpha$	<i>recA1</i> ; <i>endA1</i> ; <i>gyrA96</i> ; <i>thi</i> ; <i>relA1</i> ; <i>hsdR17</i> ( $r_{\kappa}^{-}$ , $m_{\kappa}^{+}$ ); <i>supE44</i> ; $\phi 80\Delta lacZ\Delta M15$ ; $\Delta lacZ(YA-argF)UE169$	(Sambrook et al., 1989)
<i>Escherichia coli</i> K12	Laboratory strain	ATCC 47076
<i>Escherichia coli</i> GSK1161434	Clinical isolate	GSK Microbiology Culture Collection(O'dwyer et al., 2015)
<i>Klebsiella pneumoniae</i> LMG20218	Laboratory strain	(Li et al., 2018)
<i>Mycobacterium abscessus</i> 144C	Clinical isolate	This study
<i>Mycobacterium abscessus</i> RIVM	Clinical isolate	This study
<i>Mycobacterium marinum</i> M <sup>USA</sup>	Laboratory strain	ATCC BAA-535
<i>Mycobacterium marinum</i> R-TBA161-C	M <sup>USA</sup> derivative, <i>aspS</i> <sub>R168G</sub> ( <i>mmar_2158</i> )	This study
<i>Mycobacterium tuberculosis</i> H37Rv	Laboratory strain	ATCC 25618
<i>Mycobacterium tuberculosis</i> R-TBA161-C	H37Rv derivative, <i>aspS</i> <sub>F526L</sub> ( <i>rv2572c</i> )	This study
<i>Streptococcus pneumoniae</i> D39V	Serotype 2	(Avery et al., 1944; Slager et al., 2018)

**Table S5.** Primers used in this study.

Oligonucleotide	Sequence 5'-3'
B255	ATCCGCATGCTTAATTAAGGGAGAACGTGTTTGTGCTGCGTAGCCA
B254	ATTAATTAGCTAAAGCTTATGTCCCCTCAACTTGTTGG
B256	ATCCGCATGCTTAATTAAGGGAGAACGTGTTTGTGCTGCGCAGCCA
B257	ATTAATTAGCTAAAGCTTATGCCTGCTGGACCCGCTTG
B245	CTTAGCTAATCAACTAGTGTTAACTATTTAATTGGGGACCC
B260	AATGCAGCTAGAACTAGTTCTGACCAGGGAAAATAGCCCTC
B243	AGAGAAGGCGGTATCGATATGTCGAAGGGCGAGGAGCT
B244	CTAATCAGCGGCCGCACGCGTCTACTTGTACAGCTCGTCCATGCC
B242	ATTAATTAGCTAAAGCTTACTTGTACAGCTCGTCCATGC
B241	ATCCGCATGCTTAATTAACAGAAAGGAGGTTAATAATGGTGAGCAAGGGCGA
B271	GCACGATCCGCATGCTTAATTAAGGGAGAACATGTTGCAGGGGATCGCTCG
B272	CCAATTAATTAGCTAAAGCTCTATCCACGACCACTCAGCG

**Table S6.** Plasmids used in this study.

Plasmids	Characteristics	References
pMS2	P <sub>hsp60</sub> ; oriE(CoIE1); PAL5000 origin, <i>hyg</i> <sup>R</sup> ; 5229 bp	(Kaps et al., 2001)
pMS2-tdTomato	P <sub>wmyc</sub> - <i>tdTomato</i> ; oriE(CoIE1); PAL5000 origin; <i>hyg</i> <sup>R</sup> ; 6132 bp	(Ho et al., 2021)
pMN016	P <sub>smyc</sub> - <i>mspA</i> ; ColE1 origin; PAL5000 origin; <i>hyg</i> ; 6164 bp	(Stephan et al., 2005)
pLJR965	L5 attP, <i>aph</i> <sup>R</sup> , <i>tetR</i> <sup>on</sup> , P <sub>teto</sub> - <i>Sth1 dCas9</i> , oriE, 8631 bp	(Rock et al., 2017)
pLJR965-gfp	L5 attP, <i>aph</i> <sup>R</sup> , <i>tetR</i> <sup>on</sup> , P <sub>teto</sub> - <i>mgfp2+</i> , oriE, 5909 bp	This study
pMN437	P <sub>smyc</sub> - <i>mycgfp2+</i> , oriE(CoIE1); PAL5000 origin, <i>hyg</i> <sup>R</sup> ; 6236 bp	(Song et al., 2008)
pMN437R	P <sub>smyc</sub> - <i>tdtomato</i> , oriE(CoIE1); PAL5000 origin, <i>hyg</i> <sup>R</sup> ; 6214 bp	This study
pTetDuo	PAL5000 origin, <i>hyg</i> <sup>R</sup> , <i>tetR</i> <sup>on</sup> , P <sub>teto</sub> - <i>mgfp2+</i> , P <sub>smyc</sub> - <i>tdtomato</i> , oriE, 7936bp	This study
pML2424	pUC origin; pAL5000ts; <i>sacR</i> ; <i>sacB</i> ; P <sub>wmyc</sub> - <i>tdtomato</i> ; <i>loxP</i> -P <sub>smyc</sub> - <i>mycgfp2+</i> <i>hyg</i> - <i>loxP</i> ; 9527bp	(Ofer et al., 2012)
pMS2-AspS <sub>Mmar</sub>	P <sub>smyc</sub> -AspS <sub>Mmar</sub> , oriE(CoIE1); PAL5000 origin; <i>hyg</i> <sup>R</sup> ; 7282 bp	This study
pMS2-AspS <sub>MmarR168G</sub>	P <sub>smyc</sub> -AspS <sub>MmarR168G</sub> , oriE(CoIE1); PAL5000 origin; <i>hyg</i> <sup>R</sup> ; 7282 bp	This study
pMS2-AspS <sub>Mtb</sub>	P <sub>smyc</sub> -AspS <sub>Mtb</sub> , oriE(CoIE1); PAL5000 origin; <i>hyg</i> <sup>R</sup> ; 7291 bp	This study
pMS2-AspS <sub>MtbF526L</sub>	P <sub>smyc</sub> -AspS <sub>MtbF526L</sub> , oriE(CoIE1); PAL5000 origin; <i>hyg</i> <sup>R</sup> ; 7291 bp	This study
pML1342	P <sub>wmyc</sub> - <i>xyIE</i> M; oriE(CoIE1); <i>hyg</i> <sup>R</sup> ; <i>int L5</i> ; <i>ttsbiA</i> ; <i>ttsbiB</i> ; 5404 bp	(Huff et al., 2010)
pML1342-AspS <sub>MtbF526L</sub>	P <sub>wmyc</sub> - <i>xyIE</i> M; P <sub>smyc</sub> -AspS <sub>MtbF526L</sub> ; oriE(CoIE1); <i>hyg</i> <sup>R</sup> ; <i>int L5</i> ; <i>ttsbiA</i> ; <i>ttsbiB</i> ; 7496 bp	This study
pMS2-MmpLI13 <sub>Mmar</sub>	P <sub>smyc</sub> -MmpI13 <sub>Mmar</sub> , oriE(CoIE1); PAL5000 origin; <i>hyg</i> <sup>R</sup> ; 7844 bp	This study
pMS2-MmpLI13 <sub>MmarP502R</sub>	P <sub>smyc</sub> -MmpI13 <sub>MmarP502R</sub> , oriE(CoIE1); PAL5000 origin; <i>hyg</i> <sup>R</sup> ; 7844 bp	This study



**Table S7.** Physicochemical properties of non-toxic TBA compounds and reference antibiotics.

[Click here to download Table S7](#)

## Supplementary references

- Avery, O. T., Macleod, C. M. and McCarty, M.** (1944). Studies on the chemical nature of the substance inducing transformation of pneumococcal types: Induction of transformation by a desoxyribonucleic acid fraction isolated from pneumococcus type iii. *J. Exp. Med.* **79**, 137–158.
- Backman, T. W. H., Cao, Y. and Girke, T.** (2011). ChemMine tools: An online service for analyzing and clustering small molecules. *Nucleic Acids Res.* **39**,.
- Bertz, S. H.** (2002). The first general index of molecular complexity. *J. Am. Chem. Soc.* **103**, 3599–3601.
- Hendrickson, J. B., Huang, P. and Toczko, A. G.** (1987). Molecular Complexity: A Simplified Formula Adapted to Individual Atoms. *J. Chem. Inf. Comput. Sci.* **27**, 63–67.
- Ho, V. Q. T., Verboom, T., Rong, M. K., Habjan, E., Bitter, W. and Speer, A.** (2021). Heterologous expression of ethA and katG in Mycobacterium marinum enables the rapid identification of new prodrugs active against Mycobacterium tuberculosis. *Antimicrob. Agents Chemother.* **65**,.
- Huff, J., Czyz, A., Landick, R. and Niederweis, M.** (2010). Taking phage integration to the next level as a genetic tool for mycobacteria. *Gene* **468**, 8–19.
- Kaps, I., Ehrt, S., Seeber, S., Schnappinger, D., Martin, C., Riley, L. W. and Niederweis, M.** (2001). Energy transfer between fluorescent proteins using a co-expression system in Mycobacterium smegmatis. *Gene* **278**, 115–124.
- Li, Q., Montalban-Lopez, M. and Kuipers, O. P.** (2018). Increasing the antimicrobial activity of nisinbased lantibiotics against Gram-negative pathogens. *Appl. Environ. Microbiol.* **84**,.
- O'dwyer, K., Spivak, A. T., Ingraham, K., Min, S., Holmes, D. J., Jakielaszek, C., Rittenhouse, S., Kwan, A. L., Livi, G. P., Sathe, G., et al.** (2015). Bacterial Resistance to Leucyl-tRNA Synthetase Inhibitor GSK2251052 Develops during Treatment of Complicated Urinary Tract Infections. *Antimicrob Agents Chemother.*
- Ofer, N., Wishkautzan, M., Meijler, M., Wang, Y., Speer, A., Niederweis, M. and Gur, E.** (2012). Ectoine biosynthesis in Mycobacterium smegmatis. *Appl. Environ. Microbiol.* **78**, 7483–7486.

- Rock, J. M., Hopkins, F. F., Chavez, A., Diallo, M., Chase, M. R., Gerrick, E. R., Pritchard, J. R., Church, G. M., Rubin, E. J., Sasseti, C. M., et al.** (2017). Programmable transcriptional repression in mycobacteria using an orthogonal CRISPR interference platform. *Nat. Microbiol.* **2**, 16274.
- Sambrook, J., Fritsch, E. F. and Maniatis, T.** (1989). Molecular cloning: a laboratory manual. *Mol. cloning a Lab. manual.*
- Slager, J., Aprianto, R. and Veening, J. W.** (2018). Deep genome annotation of the opportunistic human pathogen *Streptococcus pneumoniae* D39. *Nucleic Acids Res.* **46**, 9971–9989.
- Song, H., Sandie, R., Wang, Y., Andrade-Navarro, M. A. and Niederweis, M.** (2008). Identification of outer membrane proteins of *Mycobacterium tuberculosis*. *Tuberculosis* **88**, 526–544.
- Stephan, J., Bender, J., Wolschendorf, F., Hoffmann, C., Roth, E., Mailänder, C., Engelhardt, H. and Niederweis, M.** (2005). The growth rate of *Mycobacterium smegmatis* depends on sufficient porin-mediated influx of nutrients. *Mol. Microbiol.* **58**, 714–730.